STATISTICS, OPTIMIZATION AND INFORMATION COMPUTING
Stat., Optim. Inf. Comput., Vol. **x**, Month 202x, pp 0–30.
Published online in International Academic Press (www.IAPress.org)

Fractional Dynamics and Sensitivity Analysis of a Diphtheria Spread Model

Mohamad Tafrikan [1,2], Fatmawati [1,*], Windarto [1], Chinwendu E. Madubueze [3]

[1] *Department of Mathematics, Faculty of Science and Technology, Universitas Airlangga, Surabaya, 60115, East Java, Indonesia*
[2] *Department of Mathematics, Faculty of Science and Technology, Universitas Islam Negeri Walisongo Semarang, 50185, Central Java, Indonesia*
[3] *Department of Mathematics, Faculty of Science and Technology, Joseph Sarwuan Tarka University, 970101, Makurdi, Nigeria*

Abstract In this paper, we investigate a fractional compartmental model for community-level infectious disease transmission. By employing Caputo fractional derivatives, we formulate an $SEIAQR$ epidemic model. Using fixed-point theory, we establish the existence and uniqueness of solutions for the proposed system. Through a comprehensive mathematical approach, we first establish essential properties of the solutions, including non-negativity and boundedness. The basic reproduction number $\mathcal{R}_0$ is evaluated using the next-generation matrix method to determine the potential for disease spread in the community. Stability analysis, we investigate local and global stability existence by applying Matignon's theorem and constructing an appropriate Lyapunov function. The local stability for disease-free equilibrium point is proved by applying the Routh–Hurwitz criterion. For Sensitivity analysis of the basic reproduction number is conducted, elucidating the most influential model parameters. Finally, a dedicated numerical technique is applied to solve the proposed model. We also present a comparison of the root mean square error (RMSE) for different values of the fractional order α. The results show that $\alpha = 0.97$ yields a smaller RMSE, suggesting that this value should be considered by the government as a strategy to reduce diphtheria outbreaks and enhance vaccination coverage.

Keywords Fractional-order model, Diphtheria, Stability analysis, Caputo fractional derivative

AMS 2010 subject classifications 92D30, 37C60

DOI: 10.19139/soic-2310-5070-3769

1. Introduction

Diphtheria is a vaccine-preventable disease characterized by an acute bacterial infection primarily caused by Corynebacterium diphtheriae [1]. Transmission occurs primarily through respiratory droplets in the air, direct contact with infected skin lesions, or contact with contaminated surfaces [2]. Timely medical care dramatically improves survival, reducing the case fatality rate from a potential 50% in unprotected individuals to around 10% [3]. After 2–5 days of incubation, symptoms range from mild to severe, such as trouble breathing, difficulty swallowing, and a lasting cough. Severe cases can result in myocarditis, nerve damage, or kidney failure [4]. A significant hurdle in controlling outbreaks is the risk posed by infected individuals who show no symptoms but can still spread the disease for many weeks [5]. Consequently, prevention centers on vaccination, beginning with a three-dose primary series in infancy, followed by scheduled booster doses throughout childhood and adolescence [6].Therefore, public

*Correspondence to: Fatmawati (Email: fatmawati@fst.unair.ac.id). Department of Mathematics, Faculty of Science and Technology, Airlangga University, Surabaya, 60115, East Java, Indonesia.

ISSN 2310-5070 (online) ISSN 2311-004X (print)

health initiatives must prioritize educating parents on how complete immunization is critical to interrupting disease transmission [7].

Epidemiological data from 2012–2023 shows Indonesia experienced 7,886 diphtheria cases resulting in 339 deaths. Case incidence peaked in 2018 (1,386 infections), whereas mortality was highest in 2022 (46 deaths). The persistence of outbreaks is linked to suboptimal vaccination coverage under the national program, with rates as low as 29.6% in Papua and 49.6% in Aceh [8]. In addition to vaccination, the Indonesian Ministry of Health promotes a holistic preventive strategy that includes maintaining a healthy lifestyle, adequate nutrition, and proper sanitation to strengthen immunity. To understand how these measures affect disease transmission dynamics, a systematic evaluation is needed. Mathematical modeling serves as a key method in this regard, enabling the simulation of outbreak scenarios and the assessment of public health intervention effectiveness.

Mathematical modeling is the method of representing real-world systems through mathematical formulations, translating observable phenomena into equations to enable the analysis and comprehension of complex dynamics [9]. In epidemiology, mathematical models play a vital role by simulating disease spread, elucidating transmission mechanisms, and forecasting outbreaks. This offers a quantitative foundation for optimizing public health interventions and strategies [10]. The seminal Susceptible-Infected-Recovered (SIR) model by Kermack and McKendrick [11] provides a core epidemiological framework. Its development continued with Hethcote [12], who formalized it for a closed population. This modeling tradition is now standard for analyzing diphtheria's transmission dynamics.

A model-based study by Puspita et al. shows that a combination of vaccination and quarantine is an effective strategy for containing a diphtheria outbreak [13]. For this strategy to be effective, certain conditions must be met: vaccination coverage must exceed 88.4%, and the recovery rate must be at least 4%. The effectiveness of vaccination alone is supported by historical evidence from the Soviet Union in 1990, which recorded an 11.31% decrease in infections [14], and is reinforced by an epidemiological analysis from Thailand confirming that immunization is a key factor in reducing the number of cases [15, 16, 17, 18]. Meanwhile, other studies highlight the role of quarantine, where isolating exposed individuals has proven effective in curbing transmission, especially when combined with strategies to boost population immunity [19, 20]. Furthermore, increased vaccination rates also contribute significantly to reducing the rate of disease spread [21]. However, the challenge of diphtheria persistence remains a concern; SEIR modeling studies show that when reinfection plays a role in sustaining transmission, quarantine strategies alone are unable to completely halt the spread and risk causing the disease to become endemic [22].

In recent decades, fractional-order models have gained increasing attention due to their ability to capture memory effects, thereby providing a more realistic representation of biological dynamics than ordinary differential equation models [23]. These models have been widely applied in various fields, including ecology, epidemiology, and eco-epidemiology [24]. This memory property is mathematically embodied through the concept of nonlocality, whereby the solution to a system depends not only on current conditions but also on its entire past history [25]. To represent fractional derivatives, several commonly used definitions exist, namely the Riemann-Liouville, Caputo, Caputo-Fabrizio, and Atangana-Baleanu-Caputo definitions [26, 27]. Among these definitions, the Caputo derivative is most frequently chosen due to its superiority in terms of dynamic effectiveness, primarily thanks to its non-singular kernel, which has been shown to yield better performance than other definitions [28]. Nevertheless, the main challenge in fractional-order models is the difficulty of obtaining analytical solutions, especially for complex systems, making numerical approaches crucial. One effective numerical method for solving fractional differential equations with Caputo derivatives is the Polynomial Least Squares method introduced by Shakeel et al., which is known to produce highly accurate solutions while also exhibiting a fast rate of convergence [29].

The diphtheria epidemic model developed by [30] employs the Caputo fractional derivative as its framework. In their analysis, the authors focused on establishing the existence and uniqueness of solutions and performing numerical simulations, reflecting the limited literature on Caputo-based epidemiological models at the time of their work. We propose a new nonlinear fractional model to study diphtheria dynamics, employing the Caputo fractional derivative within a six-compartment framework (Susceptible, Exposed, Infected, Symptomatic Infected, Quarantined, Recovered). The objective is to investigate community transmission patterns using this numerical

approach. The study will establish the model's qualitative properties, prove the local and global asymptotic stability of its equilibrium points, and conduct a sensitivity analysis to pinpoint the parameters most critical to the reproduction number. These findings are intended to guide successful disease intervention.

2. Preliminaries

Here we explain some fundamental aspects of fractional calculus related to Caputo fractional derivative.

Definition 2.1. [31] Assume that $\alpha > 0$ and let $\mathcal{L}_1$ denote the Lebesgue space associated with the Taxicab norm. The Riemann–Liouville fractional integral of function X with order α is expressed as follows

$$\mathcal{J}_t^{\alpha} X(t) = \frac{1}{\Gamma(n)} \int_0^t (t-s)^{\alpha-1} X(s)\, ds,$$

for $t \in [0, T]$ and $\mathcal{J}_t^{\alpha} \in \mathcal{L}_1([0, T])$.

Definition 2.2. [31] For $\alpha > 0$, the Caputo fractional derivative of order α of a function $f \in C^n$ is defined as

$$D^{\alpha} f(t) = \frac{1}{\Gamma(n-\alpha)} \int_0^t \frac{f^{(n)}(s)}{(t-s)^{1+\alpha-n}}\, ds,$$

where Γ is the Gamma function and $n = \lceil \alpha \rceil$. In particular, if $0 < \alpha \leq 1$, then the expression for $D^{\alpha} f(t)$ becomes

$$D^{\alpha} f(t) = \frac{1}{\Gamma(1-\alpha)} \int_0^t \frac{f'(s)}{(t-s)^{\alpha}}\, ds.$$

Next this section, we present some lemmas, theorems, and corollary which are useful to prove the main results of our paper. We first give the comparison theorem which is useful to establish the boundedness.

Theorem 2.1. *[32, 33] Let $v(t) \in C\big([0, +\infty)\big)$, $\alpha \in (0, 1]$, $\Phi, \Psi \in \mathbb{R}$, and $\Phi \neq 0$. If $v(t)$ satisfies*

$$D_*^{\alpha} v(t) \leq -\Phi v(t) + \Psi, \quad v(0) = v_0 \in \mathbb{R},$$

then

$$v(t) \leq \left(v_0 - \frac{\Psi}{\Phi}\right) \mathcal{M}_{\alpha}(-\Phi t^{\alpha}) + \frac{\Psi}{\Phi},$$

where $\mathcal{M}_{\alpha}(k)$ is said to be the Mittag-Leffler function of one parameter and is defined by

$$\mathcal{M}_{\alpha}(k) = \sum_{j=0}^{\infty} \frac{k^j}{\Gamma(\alpha j + 1)}.$$

For the special, if $\alpha = 1$ then the equation above becomes the exponential function which has an important role in the classical calculus

$$e^k = \mathcal{M}_1(k) = \sum_{j=0}^{\infty} \frac{k^j}{\Gamma(j+1)}.$$

In [34], the correlations between the Mittag-Leffler and Wright functions are studied. The further lemma and corollary are presented to show the non-negativity of the solution in the system (2).

Lemma 2.1. *[35] Let* $\left(v, D_*^\alpha v\right)(t) \in C\left([0,\zeta]\right)$ *and* $0 < \alpha \leq 1$. *Then, one has*

$$v(t) = v(0) + \frac{1}{\Gamma(\alpha)} D_*^\alpha v(\xi)\, t^\alpha,$$

where $\xi \in [0, y]$, *for all* $y \in [0, \xi)$.

Corollary 2.1. *[35] Let* $\left(v, D_*^\alpha v\right)(t) \in C[0,\zeta]$ *and* $0 < \alpha \leq 1$. *The function* $v(t)$ *is increasing for all* $t \in (0,\zeta)$ *if* $D_*^\alpha v(t) \geq 0$, *and it is decreased for all* $t \in (0,\zeta)$ *if* $D_*^\alpha v(t) \leq 0$.

Lemma 2.2. *[36] We consider* $v(t) \in C(\mathbb{R}_+)$ *and for any* $0 < \alpha \leq 1$ *the fractional system of order* α *exist. Then, one has*

$$D_*^\alpha \left[v(t) - v^* - v^* \ln \frac{v(t)}{v^*} \right] \leq \left(1 - \frac{v^*}{v(t)}\right) D_*^\alpha v(t),$$

$v^* \in \mathbb{R}_+$, *for any* $t > 0$.

Lemma 2.3. *[37] Suppose* Ω *is a set that is bounded and closed and every solution of*

$$D^\alpha v(t) = f\big(v(t)\big),$$

start from and remain in Ω *for all time. If there exists a continuous function* $V(v) : \Omega \to \mathbb{R}$ *satisfying*

$$D^\alpha V(v)|_{D^\alpha v(t) = f(v(t))} \leq 0,$$

where $\mathcal{K}$ *is the largest set of variants of* $E := \left\{ v \;\middle|\; D^\alpha V(t)|_{D^\alpha v(t)=f(v(t))} = 0 \right\}$. *Then, for each solution* $v(t)$ *starting from* Ω *approaches to* $\mathcal{K}$ *as* $t \to \infty$.

3. Model Formulation

In this section, we describe the $SEIAQR$ biological model to study the dynamic behavior of diphtheria disease spread. The total population is divided into six compartments, namely susceptible individuals $S(t)$, exposed individuals $E(t)$, symptomatic infected individuals $I(t)$, asymptomatic infected individuals $A(t)$, quarantined infected individuals $Q(t)$, and recovered individuals $R(t)$. All of these compartments are time-dependent and the total population is given by $N(t) = S(t) + E(t) + I(t) + A(t) + Q(t) + R(t)$. The flow of infection between compartments of the model is visualized in Figure 1, and the related parameter details are presented in Table 1.

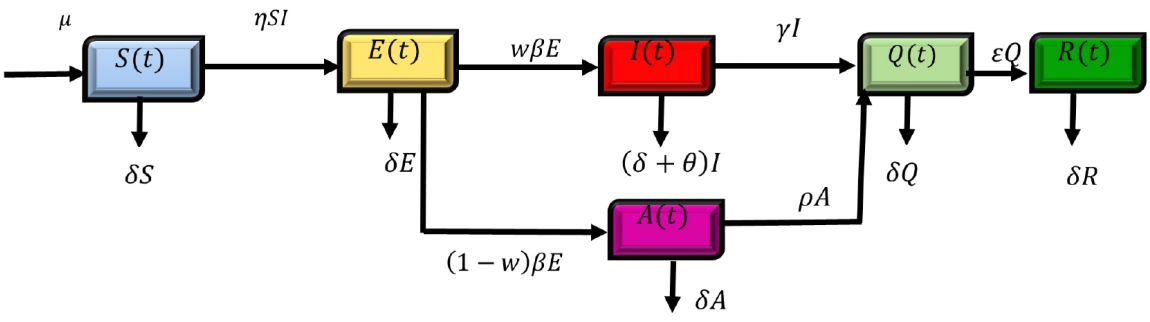

Figure 1. The compartmental structure of SEIAQR model

Table 1. Model parameters and their descriptions

Parameter	Description
w	Proportion of infected individuals who are symptomatic
μ	Natural growth rate
δ	Natural death rate
η	Interaction probability between susceptible and infected sub-populations
β	Infection (transmission) rate
γ	Quarantine rate of symptomatic infected individuals
ε	Recovery rate
θ	Disease-induced death rate due to diphtheria
ρ	Quarantine rate of asymptomatic infected individuals

The model is expressed in the form of a system of ordinary differential equations as follows:

$$\begin{cases} \dfrac{dS(t)}{dt} = \mu - (\delta + \eta I)S, \\ \dfrac{dE(t)}{dt} = \eta SI - (\beta + \delta)E, \\ \dfrac{dI(t)}{dt} = w\beta E - (\gamma + \delta + \theta)I, \\ \dfrac{dA(t)}{dt} = (1-w)\beta E - (\rho + \delta)A, \\ \dfrac{dQ(t)}{dt} = \rho A + \gamma I - (\delta + \varepsilon)Q, \\ \dfrac{dR(t)}{dt} = \varepsilon Q - \delta R. \end{cases} \tag{1}$$

It can be observed that the growth rate in model (1) only depends on the current state. In reality, however, the population growth rate is not only influenced by current conditions, but also by memory effects and long-term interactions inherent in the diphtheria transmission model, which are ignored when using integer-order derivatives. These memory effects are particularly relevant because disease transmission processes, immune responses, and population behavioral dynamics all depend on the history of previous exposures and interactions [38].

The fractional order parameter $\alpha = 0.97$ has a concrete biological interpretation in the context of diphtheria. This parameter reflects three main aspects: (i) the duration of immunity acquired from vaccination or natural infection has a long duration and affects current individual susceptibility, where a value of α close to 1 indicates that past immunity still strongly influences current susceptibility; (ii) reporting delays and the incubation period of diphtheria (2–5 days) cause current transmission events to depend on conditions from several days earlier, so the memory effect is reflected in the delay of epidemic response; and (iii) population behavioral memory, where community adherence to health protocols such as quarantine, vaccination, and mask usage is shaped by past outbreak experiences, so current preventive behavior is determined not only by current conditions but also by the history of previous interventions. Ignoring memory effects in integer-order models can lead to inaccuracies in predicting epidemic trajectories, especially during the early and late stages of an outbreak. Therefore, fractional derivatives are applied to incorporate these memory effects and long-term interactions into the biological system more realistically [38].

In this paper, we consider the Caputo fractional derivative. Since the Caputo fractional derivative of order α is the nonlocal operator (involving both the initial state and the current state), then the Caputo derivative is used in the dynamical system of model (2) to represent the influence of memory effects and long-term interactions. Thus, the growth rate in model (2) not only reflects the current conditions but also the initial conditions, so that memory effects and long-term interactions can be taken into account. The first derivative of model (2) is then replaced by the Caputo fractional derivative of order α, resulting in

$$\begin{cases} D_t^\alpha S(t) = \mu - (\delta + \eta I)S, \\ D_t^\alpha E(t) = \eta SI - (\beta + \delta)E, \\ D_t^\alpha I(t) = w\beta E - (\gamma + \delta + \theta)I, \\ D_t^\alpha A(t) = (1-w)\beta E - (\rho + \delta)A, \\ D_t^\alpha Q(t) = \rho A + \gamma I - (\delta + \varepsilon)Q, \\ D_t^\alpha R(t) = \varepsilon Q - \delta R. \end{cases} \tag{2}$$

with the initial conditions

$$S(0) = S_0 \geq 0,\ E(0) = E_0 \geq 0,\ I(0) = I_0 \geq 0,\ A(0) = A_0 \geq 0,\ Q(0) = Q_0 \geq 0,\ R(0) = R_0 \geq 0.$$

The feasible biological region for the governed model (2) is recognized as:

$$\Omega = \left\{ (S(t), E(t), I(t), A(t), Q(t), R(t)) \in \mathbb{R}_+^6 : 0 < N(t) \leq \frac{\mu}{\delta} \right\}.$$

4. Qualitative Analysis

In this section, an analysis will be conducted on the existence, uniqueness, non-negativity, and boundedness of the solutions of model (2) to ensure the validity of the model in representing real-world phenomena.

4.1. Boundedness and Non-negativity

The developed model describes the transmission mechanism among subpopulations in the dynamics of diphtheria spread. Each subpopulation is represented by dependent variables such as S, E, I, A, Q, and R. The developed model considers that the dynamics of diphtheria spread are influenced by resource constraints, such as health service capacity, food availability, and environmental carrying capacity. Therefore, each solution from the model must be limited to reflect the reality. Thus, this section examines nonnegativity, and boundedness of the solutions of model (2) to ensure that the proposed model is valid in representing the real phenomenon of diphtheria transmission.

Theorem 4.1. *Given the initial conditions*

$$\{(S(0), E(0), I(0), A(0), Q(0), R(0)) \geq 0\} \in \Omega,$$

the solutions of model (2) *are bounded in the biologically feasible region*

$$\Omega = \left\{ (S, E, I, A, Q, R) \in \mathbb{R}_+^6 : N(t) \leq \frac{\mu}{\delta} \right\}.$$

Proof
Let $N(t)$ denote the total population of the dynamical system in model (2), defined as $N(t) = S(t) + E(t) + I(t) + A(t) + Q(t) + R(t)$. Applying the fractional derivative D_t^α to both sides and summing the equations in (2), we obtain

$$\begin{aligned} D_t^\alpha N(t) &= D_t^\alpha S(t) + D_t^\alpha E(t) + D_t^\alpha I(t) + D_t^\alpha A(t) + D_t^\alpha Q(t) + D_t^\alpha R(t) \\ &= \mu - \delta N(t) - \theta I(t). \end{aligned}$$

Since $\theta > 0$ and $I(t) \geq 0$ for all $t \geq 0$, we have $-\theta I(t) \leq 0$. Hence,

$$D_t^\alpha N(t) \leq \mu - \delta N(t).$$

Based on the standard comparison theorem for fractional derivatives of order α at Theorem (2.1), $D_t^\alpha N(t) \leq \mu - N(t)\delta$ leads to

$$N(t) \leq \left(N_0 - \frac{\mu}{\delta}\right) \mathcal{M}_\alpha[-\delta t^\alpha] + \frac{\mu}{\delta},$$

where $\mathcal{M}_\alpha$ is the Mittag-Leffler function. Moreover, Lemma 5 and Corollary 6 are applied in (See [39]) to get $\mathcal{M}_\alpha[-\delta t^\alpha] \to 0$ as $t \to \infty$. As a result, we obtain

$$\limsup_{t\to\infty} N(t) \leq \frac{\mu}{\delta}.$$

□

The positivity of the solutions for the diphtheria model (2) will be verified for all non-negative initial conditions of the compartments for $t > 0$. The proof showing the non-negativity of the solutions for all state variables of the model (2) is presented below.

Theorem 4.2. *Given the initial values* $\{(S(0), E(0), I(0), A(0), Q(0), R(0)) \geq 0\} \in \varphi$ *of dynamical system of model* (2)*, the solution set* $\{S(t), E(t), I(t), A(t), Q(t), R(t)\}$ *of the system is non-negative for all* $t > 0$.

Proof
Consider $(2)_1$, one can derive

$$\begin{aligned} D_t^\alpha S(t) &= \mu - (\delta + \eta I)S, \\ &\geq -(\delta + \eta I)S \geq -\left(\delta + \frac{\eta\mu}{\delta}\right) S, \end{aligned} \tag{3}$$

which implies that

$$D_t^\alpha S(t) + \left(\delta + \frac{\eta\mu}{\delta}\right) S \geq 0.$$

By the standard comparison at Theorem (2.1), it follows that

$$\begin{aligned} S(t) &\geq -\left[(S(0) - 0)\,\mathcal{M}_\alpha\left\{-\left(\delta + \frac{\eta\mu}{\delta}\right) t^\alpha\right\} + 0\right], \\ &\geq \left[(S(0) - 0)\,\mathcal{M}_\alpha\left\{-\left(\delta + \frac{\eta\mu}{\delta}\right) t^\alpha\right\}\right], \end{aligned} \tag{4}$$

since $\mathcal{M}_\alpha\left\{-\left(\delta + \frac{\eta\mu}{\delta}\right) t^\alpha\right\} \approx 0$ as $t \to \infty$, it can be concluded that $S(t) \geq 0$. In addition, we can use a similar method to $(2)_2$, and one has

$$\begin{aligned} D_t^\alpha E(t) &= \eta SI - (\beta + \delta)E, \\ &\geq -(\beta + \delta)\,E, \end{aligned} \tag{5}$$

which gives

$$D_t^\alpha E(t) + (\beta + \delta)\,E \geq 0. \tag{6}$$

By the standard comparison at Theorem (2.1), it follows that

$$\begin{aligned} E(t) &\geq -\left[(E(0) - 0)\,\mathcal{M}_\alpha\left\{-(\beta + \delta)\,t^\alpha\right\} + 0\right], \\ &\geq \left[(E(0) - 0)\,\mathcal{M}_\alpha\left\{-(\beta + \delta)\,t^\alpha\right\}\right], \end{aligned} \tag{7}$$

Because $\mathcal{M}_\alpha\left\{-(\beta + \delta)\,t^\alpha\right\} \approx 0$ as $t \to \infty$, then the positivity of $E(t) \geq 0$ is achieved. Consequently, we have the same results for $(2)_3$, $(2)_4$, $(2)_5$, and $(2)_6$, by having $I(t) \geq I(0)\mathcal{M}_\alpha\{-(\gamma + \delta + \theta)\,t^\alpha\} \geq 0$, $A(t) \geq A(0)\mathcal{M}_\alpha\{-(\rho + \delta)t^\alpha\} \geq 0$, $Q(t) \geq Q(0)\mathcal{M}_\alpha\{-(\delta + \varepsilon)\,t^\alpha\} \geq 0$, $R(t) \geq R(0)\mathcal{M}_\alpha\{-\delta t^\alpha\} \geq 0$, and $\mathcal{M}_\alpha\left\{-(\gamma + \delta + \theta)\,t^\alpha\right\} \approx 0$, $\mathcal{M}_\alpha\left\{-(\rho + \delta)\,t^\alpha\right\} \approx 0$, $\mathcal{M}_\alpha\left\{-(\delta + \varepsilon)\,t^\alpha\right\} \approx 0$, $\mathcal{M}_\alpha\left\{-\delta t^\alpha\right\} \approx 0$ as $t \to \infty$. Then, we can conclude that $I(t) \geq 0,\ A(t) \geq 0,\ Q(t) \geq 0,\ R(t) \geq 0$. □

4.2. Existence and Uniqueness

This section discusses the existence and uniqueness of fractional dynamic system solutions (2) through maximality conditions. This existence and uniqueness are necessary to ensure that the first-order fractional system has solutions that are consistent with the given initial conditions.

Lemma 4.1. *Consider the constant ℓ_k and $\bar{\ell_k}$, such that*

$$|F_k(f_k,t) - F_k(f_k^*,t)|^2 \leq \ell_k \, |f_k - f_k^*|^2 \tag{8}$$

for all $(f,t) \in (\mathbb{R}^6 \times (0,T))$, and

$$|F_k(f_k,t)|^2 \leq \bar{\ell_k}(1 + |f_k|^2) \tag{9}$$

for all $(f,t) \in (\mathbb{R}^6 \times (0,T))$.

Inequality (8) is the Lipschitz condition, and inequality (9) is the linear growth condition. Before we prove the existence and uniqueness of our dynamical system of model (2) through (8) and (9), then as the first step, we assume that

$$\begin{aligned}
F_1(t,S,E,I,A,Q,R) &:= D_t^\alpha S(t) = \mu - (\delta + \eta I)S,\\
F_2(t,S,E,I,A,Q,R) &:= D_t^\alpha E(t) = \eta SI - (\beta + \delta)E,\\
F_3(t,S,E,I,A,Q,R) &:= D_t^\alpha I(t) = w\beta E - (\gamma + \delta + \theta)I,\\
F_4(t,S,E,I,A,Q,R) &:= D_t^\alpha A(t) = (1-w)\beta E - (\rho + \delta)A,\\
F_5(t,S,E,I,A,Q,R) &:= D_t^\alpha Q(t) = \rho A + \gamma I - (\delta + \varepsilon)Q,\\
F_6(t,S,E,I,A,Q,R) &:= D_t^\alpha R(t) = \varepsilon Q - \delta R,\\
(f_1,f_2,f_3,f_4,f_5,f_6) &:= (S,E,I,A,Q,R),\\
(f_1^*,f_2^*,f_3^*,f_4^*,f_5^*,f_6^*) &:= (S^*,E^*,I^*,A^*,Q^*,R^*).
\end{aligned} \tag{10}$$

then, we first establish the following inequality

$$|F_1(S,t) - F_1(S^*,t)|^2 \leq \ell_1 \, |S - S^*|^2 , \tag{11}$$

it follows from (10), one has

$$\begin{aligned}
|F_1(S,t) - F_1(S^*,t)|^2 &= |\mu - (\delta + \eta I)S - \mu - (\delta + \eta I)S^*|^2 ,\\
&\leq |\delta + \eta I|^2 \, |S - S^*|^2 ,\\
&\leq (\delta + |\eta I|)^2 \, |S - S^*|^2 ,\\
&\leq 2\left(\delta^2 + \eta^2 |I|^2\right) |S - S^*|^2 ,\\
&\leq 2\left(\delta^2 + \eta^2 \sup_{0\leq t\leq \kappa} |I|^2\right) |S - S^*|^2 ,\\
&\leq \ell_1 \, |S - S^*|^2 .
\end{aligned}$$

where $\ell_1 = 2\left(\delta^2 + \eta^2 \sup_{0\leq t\leq \kappa} |I|^2\right)$. In the same way, we obtain

$$\begin{aligned}
|F_2(E,t) - F_2(E^*,t)|^2 &\leq \ell_2 \, |E - E^*|^2 , \quad \ell_2 = 2\left(\beta^2 + \delta^2\right),\\
|F_3(I,t) - F_3(I^*,t)|^2 &\leq \ell_3 \, |I - I^*|^2 , \quad \ell_3 = 2\left(\gamma^2 + \delta^2 + \theta^2\right),\\
|F_4(A,t) - F_4(A^*,t)|^2 &\leq \ell_4 \, |A - A^*|^2 , \quad \ell_4 = 2\left(\rho^2 + \delta^2\right),\\
|F_5(Q,t) - F_5(Q^*,t)|^2 &\leq \ell_5 \, |Q - Q^*|^2 , \quad \ell_5 = 2\left(\delta^2 + \varepsilon^2\right),\\
|F_6(R,t) - F_6(R^*,t)|^2 &\leq \ell_6 \, |R - R^*|^2 , \quad \ell_6 = \delta^2.
\end{aligned}$$

Based on the above calculations, we can conclude that the first inequality (8) in Lemma (4.1) is satisfied. We continue to prove the second inequality (9). For F_1, assuming that $\frac{2(\delta^2+\eta^2\|I\|_\infty^2)}{\mu^2} < 1$, we obtain

$$\begin{aligned}
|F_1(S,t)|^2 &= |\mu - (\delta+\eta I)S|^2, \\
&\leq (|\mu| + |(\delta+\eta I)S|)^2, \\
&\leq 2\left(\mu^2 + 2\left(\delta^2 + \eta^2 \sup_{0\leq t\leq\kappa}|I|^2\right)|S|^2\right), \\
&\leq 2\mu^2 + 4\left(\delta^2+\eta^2\|I\|_\infty^2\right)|S|^2, \\
&\leq \bar{\ell_1}(1+|S|^2),
\end{aligned}$$

where $\bar{\ell_1} = 2\mu^2$. Applying the same strategy for F_2, assuming that $\frac{(\beta+\delta)^2}{(\eta^2\|S\|_\infty^2\|I\|_\infty^2)} < 1$, we obtain

$$\begin{aligned}
|F_2(E,t)|^2 &= |\eta SI - (\beta+\delta)E|^2, \\
&\leq (|\eta SI| + |(\beta+\delta)E|)^2, \\
&\leq 2\left(\eta^2 \sup_{0\leq t\leq\kappa}|S|^2 \sup_{0\leq t\leq\kappa}|I|^2 + (\beta+\delta)^2|E|^2\right), \\
&\leq 2\left(\eta^2\|S\|_\infty^2\|I\|_\infty^2 + (\beta+\delta)^2|E|^2\right), \\
&\leq 2\left(\eta^2\|S\|_\infty^2\|I\|_\infty^2\right) + 2(\beta+\delta)^2|E|^2, \\
&\leq \bar{\ell_2}(1+|E|^2),
\end{aligned}$$

with $\bar{\ell_2} = 2\left(\eta^2\|S\|_\infty^2\|I\|_\infty^2\right)$. Furthermore, for F_3, assuming that $\frac{(\gamma+\delta+\theta)^2}{w^2\beta^2\|E\|_\infty^2} < 1$, we obtain

$$\begin{aligned}
|F_3(I,t)|^2 &= |w\beta E - (\gamma+\delta+\theta)I|^2, \\
&\leq (|w\beta E| + |(\gamma+\delta+\theta)I|)^2, \\
&\leq 2\left(w^2\beta^2 \sup_{0\leq t\leq\kappa}|E|^2 + (\gamma+\delta+\theta)^2|I|^2\right), \\
&\leq 2\left(w^2\beta^2\|E\|_\infty^2 + (\gamma+\delta+\theta)^2|I|^2\right), \\
&\leq 2w^2\beta^2\|E\|_\infty^2(1+|I|^2), \\
&\leq \bar{\ell_3}(1+|I|^2),
\end{aligned}$$

with $\bar{\ell_3} = 2w^2\beta^2\|E\|_\infty^2$. For F_4, assuming that $\frac{(\rho+\delta)^2}{(1-w)^2\beta^2\|E\|_\infty^2} < 1$, we obtain

$$\begin{aligned}
|F_4(A,t)|^2 &= |(1-w)\beta E - (\rho+\delta)A|^2, \\
&\leq (|(1-w)\beta E| + |(\rho+\delta)A|)^2, \\
&\leq 2\left((1-w)^2\beta^2 \sup_{0\leq t\leq\kappa}|E|^2 + (\rho+\delta)^2|A|^2\right), \\
&\leq 2\left((1-w)^2\beta^2\|E\|_\infty^2 + (\rho+\delta)^2|A|^2\right), \\
&\leq 2(1-w)^2\beta^2\|E\|_\infty^2(1+|A|^2), \\
&\leq \bar{\ell_4}(1+|A|^2),
\end{aligned}$$

with $\bar{\ell}_4 = 2(1-w)^2\beta^2\|E\|_\infty^2$. Next, For F_5, assuming that $\frac{(\delta+\varepsilon)^2}{\gamma^2\|I\|_\infty^2+\rho^2\|A\|_\infty^2} < 1$, we obtain

$$\begin{aligned}
|F_5(Q,t)|^2 &= |\rho A + \gamma I - (\delta+\varepsilon)Q|^2, \\
&\leq \left(|\rho A| + |\gamma I| + |(\delta+\varepsilon)Q|\right)^2, \\
&\leq 2\left(\rho^2 \sup_{0\leq t\leq\kappa}|A|^2 + \gamma^2 \sup_{0\leq t\leq\kappa}|I|^2 + (\delta+\varepsilon)^2|Q|^2\right), \\
&\leq 2\left(\rho^2\|A\|_\infty^2 + \gamma^2\|I\|_\infty^2 + (\delta+\varepsilon)^2|Q|^2\right), \\
&\leq 2\left(\rho^2\|A\|_\infty^2 + \gamma^2\|I\|_\infty^2\right)(1+|Q|^2), \\
&\leq \bar{\ell}_5(1+|Q|^2),
\end{aligned}$$

with $\bar{\ell}_5 = 2\left(\rho^2\|A\|_\infty^2 + \gamma^2\|I\|_\infty^2\right)$. Finally, for F_6, assuming that $\frac{\delta^2}{\varepsilon^2\|Q\|_\infty^2} < 1$, we obtain

$$\begin{aligned}
|F_6(R,t)|^2 &= |\varepsilon Q - \delta R|^2, \\
&\leq \left(|\varepsilon Q| + |\delta R|\right)^2, \\
&\leq 2\left(\varepsilon^2 \sup_{0\leq t\leq\kappa}|Q|^2 + \delta^2|R|^2\right), \\
&\leq 2\left(\varepsilon^2\|Q\|_\infty^2 + \delta^2|R|^2\right), \\
&\leq 2\varepsilon^2\|Q\|_\infty^2(1+|R|^2), \\
&\leq \bar{\ell}_6(1+|R|^2),
\end{aligned}$$

with $\bar{\ell}_6 = 2\varepsilon^2\|Q\|_\infty^2$.

Finally, the second inequality (9) can be established in the following maximality condition

$$\varrho = \max\left\{\frac{2(\delta^2+\eta^2\|I\|_\infty^2)}{\mu^2}, \frac{(\beta+\delta)^2}{\eta^2\|S\|_\infty^2\|I\|_\infty^2}, \frac{(\gamma+\delta+\theta)^2}{w^2\beta^2\|E\|_\infty^2}, \frac{(\rho+\delta)^2}{(1-w)^2\beta^2\|E\|_\infty^2}, \frac{(\delta+\varepsilon)^2}{\gamma^2\|I\|_\infty^2+\rho^2\|A\|_\infty^2}, \frac{\delta^2}{\varepsilon^2\|Q\|_\infty^2}\right\} < 1.$$

The maximality condition ($\varrho < 1$) is a sufficient condition for the *linear growth condition* (the second inequality in (9)) to hold. Thus, the integral operator we have defined is contractive. By the Picard-Lindelöf theorem (see [40]), this guarantees the existence and uniqueness of a solution to the model (2) for any initial conditions.

5. Equilibrium Analysis

5.1. Disease-free and Endemic Equilibria

In this section, we determine the equilibrium points of the proposed Caputo fractional-order system. There are two types of equilibrium points: the disease-free equilibrium point and the endemic equilibrium point. The disease-free equilibrium point is denoted by $\varepsilon_0 = (S_0, E_0, I_0, A_0, Q_0, R_0)$. To find this equilibrium, we set $E = I = A = Q = R = 0$ and solve for S, yielding $S_0 = \frac{\mu}{\delta}$. Thus, we obtain

$$\varepsilon_0 = (S_0, E_0, I_0, A_0, Q_0, R_0) = \left(\frac{\mu}{\delta}, 0, 0, 0, 0, 0\right).$$

The endemic equilibrium point, denoted by $\varepsilon^* = (S^*, E^*, I^*, A^*, Q^*, R^*)$, is obtained by setting the right-hand side of the fractional-order model (FOM) (2) to zero.

$$\begin{aligned}
\mu - (\delta + \eta I)S &= 0,\\
\eta SI - (\beta + \delta)E &= 0,\\
w\beta E - (\gamma + \delta + \theta)I &= 0,\\
(1-w)\beta E - (\rho + \delta)A &= 0,\\
\rho A + \gamma I - (\delta + \varepsilon)Q &= 0,\\
\varepsilon Q - \delta R &= 0.
\end{aligned}$$

where

$$S^* = \frac{\mu}{\delta + \delta(\mathcal{R}_0 - 1)}, E^* = \frac{\mu(\mathcal{R}_0 - 1)}{\mathcal{R}_0(\beta + \delta)}, I^* = \frac{\delta(\mathcal{R}_0 - 1)}{\eta}, A^* = \frac{(1-w)\beta\mu(\mathcal{R}_0 - 1)}{\mathcal{R}_0(\rho + \delta)(\beta + \delta)},$$

$$Q^* = \frac{(\mathcal{R}_0 - 1)\left[\rho(1-w)\beta\mu\eta + \gamma\delta\mathcal{R}_0(\rho + \delta)(\beta + \delta)\right]}{\mathcal{R}_0\eta(\rho + \delta)(\beta + \delta)(\delta + \varepsilon)}, R^* = \frac{\varepsilon(\mathcal{R}_0 - 1)\left[\rho(1-w)\beta\mu\eta + \gamma\delta\mathcal{R}_0(\rho + \delta)(\beta + \delta)\right]}{\delta\mathcal{R}_0\eta(\rho + \delta)(\beta + \delta)(\delta + \varepsilon)}.$$

5.2. Basic Reproduction Number

When examining the prospects or dynamics of any infection, a threshold parameter called the basic reproduction number ($\mathcal{R}_0$) is very important. An outbreak will begin as soon as an infected individual appears within a group where the entire system is vulnerable. General estimates regarding new infections caused by a clinical disease are usually given by $\mathcal{R}_0$. We evaluate $\mathcal{R}_0$ using the next-generation matrix technique for the structured model (2), and the next-generation matrix method is carried out as follows:

$$J(\xi) = F - V,$$

where $\xi = (E, I, A)$, $F(\xi) = \begin{pmatrix} \eta SI \\ 0 \\ 0 \end{pmatrix}$, and $V(\xi) = \begin{pmatrix} (\beta + \delta)E \\ -(w\beta E) + (\gamma + \delta + \theta)I \\ -(1-w)\beta E + (\rho + \delta)A \end{pmatrix}$.

The Jacobian matrices of F and V at the infection-free steady state ε_0 are given by:

$$\bar{F} = \begin{bmatrix} 0 & \frac{\eta\mu}{\delta} & 0 \\ 0 & 0 & 0 \\ 0 & 0 & 0 \end{bmatrix} \quad \text{and} \quad \bar{V} = \begin{bmatrix} \beta + \delta & 0 & 0 \\ -w\beta & \gamma + \delta + \theta & 0 \\ -(1-w)\beta & 0 & \rho + \delta \end{bmatrix}.$$

The dominant eigenvalue of the matrix product $\bar{F}\bar{V}^{-1}$ is $\mathcal{R}_0$ and is given by

$$\mathcal{R}_0 = \frac{\eta\mu w\beta}{\delta(\beta + \delta)(\gamma + \delta + \theta)}.$$

6. Local Stability Analysis

This section examines the local stability of the equilibrium points by linearizing the model (2) around the equilibrium point, which has the Jacobian matrix

$$J = \begin{bmatrix} -(\delta+\eta I) & 0 & -\eta S & 0 & 0 & 0 \\ \eta I & -(\beta+\delta) & \eta S & 0 & 0 & 0 \\ 0 & w\beta & -(\gamma+\delta+\theta) & 0 & 0 & 0 \\ 0 & (1-w)\beta & 0 & -(\rho+\delta) & 0 & 0 \\ 0 & 0 & \gamma & \rho & -(\delta+\varepsilon) & 0 \\ 0 & 0 & 0 & 0 & \varepsilon & -\delta \end{bmatrix}. \tag{12}$$

To analyze the local stability of the equilibrium points, the Jacobian matrix of the system is evaluated at the corresponding equilibrium. According to the stability criterion for fractional-order systems of order α given by [41, 42], an equilibrium point is asymptotically stable if all eigenvalues λ_i of the Jacobian matrix satisfy the condition $|\arg(\lambda_i)| > \frac{\alpha\pi}{2}$. This criterion, known as the Matignon condition, is applied to the eigenvalues obtained from the Jacobian matrix at the disease-free and endemic equilibrium points to determine their stability.

6.1. The Free Disease Equilibrium Point

In this section, the local stability analysis of model (2) is mentioned at disease-free [43] $\varepsilon_0 = (S_0, E_0, I_0, A_0, Q_0, R_0) = (\frac{\mu}{\delta}, 0, 0, 0, 0, 0)$. The Jacobian matrix (12) evaluated at ε_0 is then determined as follows:

$$J(\varepsilon_0) = \begin{bmatrix} -\delta & 0 & -\frac{\eta\mu}{\delta} & 0 & 0 & 0 \\ 0 & -(\beta+\delta) & \frac{\eta\mu}{\delta} & 0 & 0 & 0 \\ 0 & w\beta & -(\gamma+\delta+\theta) & 0 & 0 & 0 \\ 0 & (1-w)\beta & 0 & -(\rho+\delta) & 0 & 0 \\ 0 & 0 & \gamma & \rho & -(\delta+\varepsilon) & 0 \\ 0 & 0 & 0 & 0 & \varepsilon & -\delta \end{bmatrix}, \tag{13}$$

we now demonstrate the critical assumption for the $SEIAQR$ epidemic models local stability at disease-free equilibrium point.

Theorem 6.1. *If $\mathcal{R}_0 < 1$, the suggested model (2) is considered to be locally asymptotically stable at disease-free equilibrium point ε_0, while the model is unstable if $\mathcal{R}_0 > 1$.*

Proof
We have the Jacobian matrix at ε_0 equation (13). By using cofactor expansion method, we see that the Jacobian matrix $J(\varepsilon_0)$ has the following eigenvalues

$$\lambda_1 = \lambda_2 = -\delta, \tag{14}$$
$$\lambda_3 = -\delta - \varepsilon, \tag{15}$$
$$\lambda_4 = -\delta - \rho, \tag{16}$$

the other eigenvalues are determined from the following characteristic equation:

$$\lambda^2 + m_1\lambda + m_0 = 0, \tag{17}$$

with

$$m_1 = (\gamma+\delta+\theta) + (\delta+\beta),$$
$$m_0 = (\gamma+\delta+\theta)(\delta+\beta)(1-\mathcal{R}_0).$$

From equations (14), (15), and (16), we obtain $\lambda_1 = \lambda_2 = -\delta$, $\lambda_3 = -\delta - \varepsilon$, and $\lambda_4 = -\delta - \rho$. Since all parameters $\delta, \varepsilon, \rho$ are positive, we have $\lambda_i < 0$ for $i = 1, 2, 3, 4$, which implies $|\arg(\lambda_i)| = \pi > \frac{\alpha\pi}{2}$. Consequently, the equilibrium point is asymptotically stable. By equation (17), based on the modified Routh-Hurwitz criterion

for fractional-order systems, all roots of (17) have negative real parts if and only if $m_1 > 0$ and $m_0 > 0$. Since all parameters are positive, the condition $m_1 > 0$ is always satisfied. Furthermore, $m_0 > 0$ holds if and only if $\mathcal{R}_0 < 1$. Consequently, for the remaining eigenvalues λ_5 and λ_6, we have $|\arg(\lambda_i)| = \pi > \frac{\alpha\pi}{2}$ for $i = 5, 6$ whenever $\mathcal{R}_0 < 1$, which guarantees the local asymptotic stability of the equilibrium ε_0. Conversely, if $\mathcal{R}_0 > 1$, then $m_0 < 0$, implying that the characteristic equation (17) has at least one root with a positive real part. Hence, the equilibrium ε_0 is unstable when $\mathcal{R}_0 > 1$. □

6.2. The Endemic Equilibrium Point

The Jacobian matrix (12) evaluated at ε^* is given as follows:

$$J(\varepsilon^*) = \begin{bmatrix} -(\delta + \eta I^*) & 0 & -\frac{\eta\mu}{\delta + \eta I^*} & 0 & 0 & 0 \\ \eta I^* & -(\beta + \delta) & \frac{\eta\mu}{\delta + \eta I^*} & 0 & 0 & 0 \\ 0 & w\beta & -(\gamma + \delta + \theta) & 0 & 0 & 0 \\ 0 & (1-w)\beta & 0 & -(\rho + \delta) & 0 & 0 \\ 0 & 0 & \gamma & \rho & -(\delta + \varepsilon) & 0 \\ 0 & 0 & 0 & 0 & \varepsilon & -\delta \end{bmatrix}. \tag{18}$$

Now, the following important results for the local stability analysis of the epidemiological model at the endemic equilibrium point are presented.

Theorem 6.2. *The model (2) is locally asymptotically stable at the endemic equilibrium point of ε^* if $\mathcal{R}_0 > 1$, but the system will be unstable if it is $\mathcal{R}_0 < 1$.*

Proof
The Jacobian matrix of the model (2) at $\varepsilon^* = (S^*, E^*, I^*, A^*, Q^*, R^*)$ is evaluated. The eigenvalue of the Jacobian matrix $J(\varepsilon^*)$ (18) has been determined and given as follows:

$$\lambda_1 = -\delta, \quad \lambda_2 = -(\delta + \varepsilon), \quad \lambda_3 = -(\rho + \delta).$$

Since $\delta, \varepsilon, \rho > 0$, then all of these eigenvalues have a negative real part. Hence, the eigenvalues satisfy $|\arg(\lambda_i)| = \pi > \frac{\alpha\pi}{2}$ for all $i = 1, 2, 3$, which is a stable region of equilibrium point. The other eigenvalues are determined from the following characteristic equation

$$\lambda^3 + b_1\lambda^2 + b_2\lambda + b_3 = 0, \tag{19}$$

with

$$b_1 = \theta + \gamma + \delta\mathcal{R}_0 + \beta + 2\delta,$$
$$b_2 = \delta\mathcal{R}_0(\beta + \theta + 2\delta + \gamma),$$
$$b_3 = \delta(\beta + \delta)(\gamma + \theta + \delta)(\mathcal{R}_0 - 1).$$

Based on the Routh–Hurwitz criterion for third order polynomial, the system with characteristic equation (19) is stable at the equilibrium point ε^* if $b_1 > 0$, $b_2 > 0$, $b_3 > 0$ and $b_1 b_2 > b_3$. Based on equation (19), it can be shown that $b_1 > 0$, $b_2 > 0$ and $b_3 > 0$ if $\mathcal{R}_0 > 1$. Therefore, the condition $b_1 b_2 - b_3 > 0$ is equivalent to

$$\delta\Big[\delta\mathcal{R}_0^2\Big(\beta + 2\delta\Big) + \mathcal{R}_0\Big(\beta^2 + \theta^2 + \gamma^2 + \beta\theta + \beta\gamma + 2\theta\gamma + 3\delta^2 + 3\beta\delta + 4\theta\delta + 4\gamma\delta\Big) + \mathcal{R}_0(\mathcal{R}_0 - 1)\Big(\delta\gamma + \delta\theta\Big)$$
$$+ (\beta + \delta)(\gamma + \theta + \delta)\Big] > 0.$$

Hence, $b_1 b_2 - b_3 > 0$ is satisfied only if $\mathcal{R}_0 > 1$. Thus, all Routh–Hurwitz criteria are satisfied, so all eigenvalues have negative real parts, and hence $|\arg(\lambda_i)| = \pi > \frac{\alpha\pi}{2}$ for all $i = 1, 2, 3$. Therefore, the endemic equilibrium point is locally asymptotically stable if $\mathcal{R}_0 > 1$. □

7. Global Stability Analysis

7.1. The Disease-free Equilibrium Point

The Theorem (7.1) will be proven based on the method of the Goh-Volterra lyapunov function to demonstrate the global stability of the disease-free steady state. Based on this method, the system of equation (2) is written as follows: Suppose

$$\Omega_0 = \{M \in \Omega : E = I = A = Q = R = 0\},$$

with $M = (S(t), E(t), I(t), A(t), Q(t), R(t))$. The global stability of disease-free equilibrium is given in the following theorem.

Theorem 7.1. *The disease-free equilibrium* (ε_0) *in special case is globally asymptotically stable in the interior of* $\Omega \setminus \Omega_0$ *if* $\mathcal{R}_0 < 1$.

Proof
We use Goh-Volterra type Lyapunov function $\mathcal{L}_0 : \Omega \setminus \Omega_0 \to \mathbb{R}$:

$$\mathcal{L}_0 = (S - S_0 \ln S) + E + I + A + Q + R.$$

by differentiating $\mathcal{L}_0$ with respect to time, we have

$$D_t^\alpha \mathcal{L} = \left(1 - \frac{S_0}{S}\right) D_t^\alpha S + D_t^\alpha E + D_t^\alpha I + D_\alpha A + D_t^\alpha Q + D_t^\alpha R.$$

utilizing the values from the fractional order model (2), we get

$$\begin{aligned} D_t^\alpha \mathcal{L}_0 = &\left(1 - \frac{S_0}{S}\right)[\mu - (\delta + \eta I)S] + [\eta SI - (\beta + \delta)E] + [w\beta E - (\gamma + \delta + \theta)I] + [(1-w)\beta E - (\rho + \delta)A] \\ &+ [\rho A + \gamma I - (\delta + \varepsilon)Q] + [\varepsilon Q - \delta R], \end{aligned}$$

implies that

$$D_t^\alpha \mathcal{L}_0 = \left[-\delta \frac{(S - S_0)^2}{S} + \eta I S_0 - \delta[E + I + A + Q + R] - \theta I\right]. \tag{20}$$

It is clear that $D_t^\alpha \mathcal{L}_0 \leq 0$, with $D_t^\alpha \mathcal{L}_0 = 0$ if and only if $S = S_0$, $E = I = A = Q = R = 0$. Therefore, according to La Salle's invariance principle [44], the disease-free equilibrium ε_0 is globally asymptotically stable in $\Omega \setminus \Omega_0$. Consequently, the infection dies out from the community. □

7.2. The Endemic Equilibrium Point

In this subsection, we analyze the global asymptotic stability of the endemic equilibrium of system (2). For that purpose, the invariant set Ω_0 is first defined as follows. Suppose

$$\Omega_0 = \{M \in \Omega : E = I = A = Q = 0\},$$

with $M = (S(t), E(t), I(t), A(t), Q(t), R(t))$. The global stability of endemic equilibrium is given in the following theorem.

Theorem 7.2. *The endemic equilibrium* (ε^*) *in special case is globally asymptotically stable in the interior of* $\Omega \setminus \Omega_0$ *if* $\mathcal{R}_0 > 1$.

Proof
We use Goh-Volterra type Lyapunov function $\mathcal{L} : \Omega \setminus \Omega_0 \to \mathbb{R}$:

$$\mathcal{L} = \left(S - S^* - S^* \ln \frac{S}{S^*}\right) + \left(E - E^* - E^* \ln \frac{E}{E^*}\right) + \left(I - I^* - I^* \ln \frac{I}{I^*}\right) + \left(A - A^* - A^* \ln \frac{A}{A^*}\right) + \left(Q - Q^* - Q^* \ln \frac{Q}{Q^*}\right).$$

The time derivative of $\mathcal{L}$ is

$$D_t^\alpha \mathcal{L} = \left(1 - \frac{S^*}{S}\right) D_t^\alpha S + \left(1 - \frac{E^*}{E}\right) D_t^\alpha E + \left(1 - \frac{I^*}{I}\right) D_t^\alpha I + \left(1 - \frac{A^*}{A}\right) D_t^\alpha A + \left(1 - \frac{Q^*}{Q}\right) D_t^\alpha Q. \quad (21)$$

Subtituted model (2) into equation (21) we get

$$D_t^\alpha \mathcal{L} = \left(1 - \frac{S^*}{S}\right)[\mu - (\delta + \eta I)S] + \left(1 - \frac{E^*}{E}\right)[\eta SI - (\beta + \delta)E] + \left(1 - \frac{I^*}{I}\right)[w\beta E - (\gamma + \delta + \theta)I] + \left(1 - \frac{A^*}{A}\right)[(1-w)\beta E - (\rho + \delta)A] + \left(1 - \frac{Q^*}{Q}\right)[\rho A + \gamma I - (\delta + \varepsilon)Q]. \quad (22)$$

At the equilibrium state, the model (2) yields the following relationship:

$$\mu = (\delta + \eta I^*)S^*, (\beta + \delta) = \frac{\eta S^* I^*}{E^*}, (\gamma + \delta + \theta) = \frac{w\beta E^*}{I^*}, (\rho + \delta) = \frac{(1-w)\beta E^*}{A^*}, (\delta + \varepsilon) = \frac{\rho A^* + \gamma I^*}{Q^*}. \quad (23)$$

Using the steady-state relation (23) in equation (22) and after some simplification we have:

$$\begin{aligned} D_t^\alpha \mathcal{L} = & -\delta \frac{(S - S^*)^2}{S} + \eta I^* \left[\left(3 - \frac{S^*}{S} - \frac{IS}{I^* S^*} - \frac{I^*}{I}\right) - \left(2 - \frac{I^*}{I} - \frac{I}{I^*}\right)\right] \\ & + \eta S^* I^* \left[\left(3 - \frac{SIE^*}{S^* I^* E} - \frac{E}{E^*} - \frac{S^* I^*}{SI}\right) - \left(2 - \frac{SI}{S^* I^*} - \frac{S^* I^*}{SI}\right)\right] \\ & + w\beta E^* \left[\left(3 - \frac{EI^*}{E^* I} - \frac{I}{I^*} - \frac{E^*}{E}\right) - \left(2 - \frac{E^*}{E} - \frac{E}{E^*}\right)\right] \\ & + (1-w)\beta E^* \left[\left(3 - \frac{EA^*}{E^* A} - \frac{A}{A^*} - \frac{E^*}{E}\right) - \left(2 - \frac{E^*}{E} - \frac{E}{E^*}\right)\right] \\ & + \rho A^* \left[\left(3 - \frac{AQ^*}{A^* Q} - \frac{Q}{Q^*} - \frac{A^*}{A}\right) - \left(2 - \frac{A}{A^*} - \frac{A^*}{A}\right)\right] \\ & + \gamma I^* \left[\left(3 - \frac{IQ^*}{I^* Q} - \frac{Q}{Q^*} - \frac{I^*}{I}\right) - \left(2 - \frac{I}{I^*} - \frac{I^*}{I}\right)\right] \\ & + \varepsilon Q^* \left[\left(3 - \frac{QR^*}{Q^* R} - \frac{R}{R^*} - \frac{Q^*}{Q}\right) - \left(2 - \frac{Q}{Q^*} - \frac{Q^*}{Q}\right)\right]. \end{aligned}$$

Given that the arithmetic mean is always greater than or equal to the geometric mean, implies:

$$\frac{I}{I^*} + \frac{I^*}{I} \geq 2, \frac{E}{E^*} + \frac{E^*}{E} \geq 2, \frac{A}{A^*} + \frac{A^*}{A} \geq 2, \frac{Q}{Q^*} + \frac{Q^*}{Q} \geq 2, \frac{SI}{S^* I^*} + \frac{S^* I^*}{SI} \geq 2, \frac{S^*}{S} + \frac{IS}{I^* S^*} + \frac{I^*}{I} \geq 3,$$
$$\frac{SIE^*}{S^* I^* E} + \frac{E}{E^*} + \frac{S^* I^*}{SI} \geq 3, \frac{EI^*}{E^* I} + \frac{I}{I^*} + \frac{E^*}{E} \geq 3, \frac{EA^*}{E^* A} + \frac{A}{A^*} + \frac{E^*}{E} \geq 3, \frac{AQ^*}{A^* Q} + \frac{Q}{Q^*} + \frac{A^*}{A} \geq 3,$$
$$\frac{IQ^*}{I^* Q} + \frac{Q}{Q^*} + \frac{I^*}{I} \geq 3, \frac{QR^*}{Q^* R} + \frac{R}{R^*} + \frac{Q^*}{Q} \geq 3.$$

and $(S-S^*)^2 \geq 0$, also $S \geq 0$. Hence, it is clear that

$$
\begin{aligned}
&-\delta\frac{(S-S^*)^2}{S} \leq 0, \eta I^*\left[\left(3-\frac{S^*}{S}-\frac{IS}{I^*S^*}-\frac{I^*}{I}\right)-\left(2-\frac{I^*}{I}-\frac{I}{I^*}\right)\right] \leq 0,\\
&\eta S^*I^*\left[\left(3-\frac{SIE^*}{S^*I^*E}-\frac{E}{E^*}-\frac{S^*I^*}{SI}\right)-\left(2-\frac{SI}{S^*I^*}-\frac{S^*I^*}{SI}\right)\right] \leq 0,\\
&w\beta E^*\left[\left(3-\frac{EI^*}{E^*I}-\frac{I}{I^*}-\frac{E^*}{E}\right)-\left(2-\frac{E^*}{E}-\frac{E}{E^*}\right)\right] \leq 0,\\
&(1-w)\beta E^*\left[\left(3-\frac{EA^*}{E^*A}-\frac{A}{A^*}-\frac{E^*}{E}\right)-\left(2-\frac{E^*}{E}-\frac{E}{E^*}\right)\right] \leq 0,\\
&\rho A^*\left[\left(3-\frac{AQ^*}{A^*Q}-\frac{Q}{Q^*}-\frac{A^*}{A}\right)-\left(2-\frac{A}{A^*}-\frac{A^*}{A}\right)\right] \leq 0,\\
&\gamma I^*\left[\left(3-\frac{IQ^*}{I^*Q}-\frac{Q}{Q^*}-\frac{I^*}{I}\right)-\left(2-\frac{I}{I^*}-\frac{I^*}{I}\right)\right] \leq 0,\\
&\varepsilon Q^*\left[\left(3-\frac{QR^*}{Q^*R}-\frac{R}{R^*}-\frac{Q^*}{Q}\right)-\left(2-\frac{Q}{Q^*}-\frac{Q^*}{Q}\right)\right] \leq 0.
\end{aligned}
$$

Clear that $D_t^\alpha \mathcal{L} \leq 0$, with $D_t^\alpha \mathcal{L} = 0$ if and only if $S = S^*,\ E = E^*,\ I = I^*,\ A = A^*,\ Q = Q^*$, and $R = R^*$. The endemic equilibrium point ε^* is special and unique if $\mathcal{R}_0 > 1$, and the singleton set ε^* is the largest compact invariant set in $\{(S(t), E(t), I(t), A(t), Q(t)\ , R(t)) \in \Omega : {}^C D_t^\alpha \mathcal{L} = 0\}$. Based on La Salle's invariance principle [44], ε^* is globally asymptotically stable in the interior of region $(\Omega \setminus \Omega_0)$ if $\mathcal{R}_0 > 1$. □

8. Sensitivity Analysis of Model Parameters

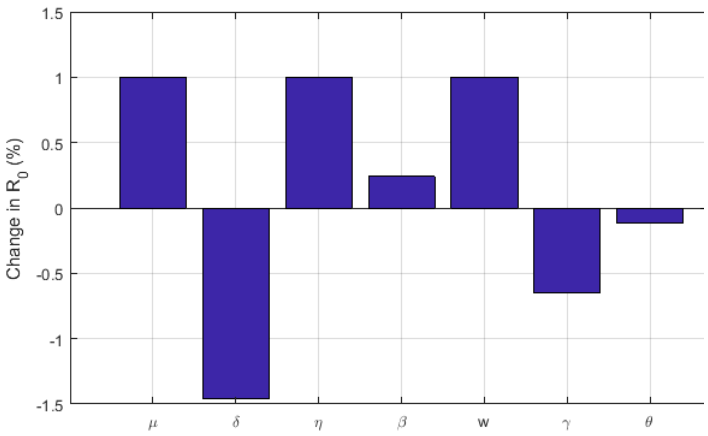

Figure 2. Sensitivity of Parameters towards $\mathcal{R}_0$

Based on the sensitivity analysis results shown in Figure 2, we can understand which parameters have the most significant impact on the spread of diphtheria. This sensitivity analysis measures how much change in a parameter, such as birth rate, death rate, or contact rate affects the change in the number of diphtheria cases. The higher the sensitivity value (both positive and negative), the greater the influence of that parameter. The sensitivity index for each parameter was calculated using the equation $\Gamma_m = \frac{\partial \mathcal{R}_0}{\partial m}\frac{m}{\mathcal{R}_0}$, where m is the parameter being analyzed. This index measures the relative change in $\mathcal{R}_0$ resulting from a small change in parameter m. A positive value indicates that an increase in the parameter will increase $\mathcal{R}_0$, while a negative value indicates the opposite.To quantify the

uncertainty in these estimates, we provide 95% confidence intervals for each sensitivity index, as shown in Table 2. The following table shows the sensitivity values for each parameter:

Table 2. Parameter Values and Sensitivity Indices of the Model

Notation	Sensitivity Index	CI Lower 95%	CI Upper 95%
μ	1	0.99	1.01
δ	-1.4603	-1.4749	-1.4457
η	1	0.99	1.01
w	1	0.99	1.01
β	0.241	0.2386	0.2434
γ	-0.6487	-0.6552	-0.6422
θ	-0.11	-0.1111	-0.1089

From Table 2 above, the natural death rate (δ) exhibits the largest sensitivity index (-1.4603%). Mathematically, an increase in δ leads to a decrease in $\mathcal{R}_0$ because a higher natural death rate accelerates the removal of susceptible individuals from the population. However, from an epidemiological perspective, this parameter is not a modifiable intervention target for disease control. This parameter reflects demographic characteristics such as age structure and population turnover. Demography influences transmission dynamics through age structure, which determines contact patterns and susceptibility, as well as through birth rate, which regulates the inflow of new susceptible individuals. This finding indicates that population characteristics need to be considered in health program planning, while control strategies should focus on parameters that can be directly intervened upon.

Parameters such as the contact rate (η) have a positive sensitivity index of $+1.0\%$. Mathematically, this positive value means that $\mathcal{R}_0$ is an increasing function of η, so that any increase in the contact rate will cause a proportional increase in $\mathcal{R}_0$, and conversely any decrease in the contact rate will decrease $\mathcal{R}_0$. This large influence indicates that small changes in the contact rate will produce significant changes in $\mathcal{R}_0$, so that interventions aimed at reducing contact between individuals are the most effective strategy for suppressing the spread of diphtheria.

Meanwhile, the quarantine rate (γ) has a negative sensitivity index of -0.6487 (95% CI: -0.6552 to -0.6422), which mathematically means that $\mathcal{R}_0$ is inversely related to γ. Any increase in the quarantine rate will decrease $\mathcal{R}_0$, while any decrease in the quarantine rate will increase $\mathcal{R}_0$. Thus, mathematically, quarantine is proven to be effective in suppressing the spread of diphtheria. However, the magnitude of the index indicates that the influence of the quarantine rate on $\mathcal{R}_0$ is relatively low compared to parameters such as the contact rate ($\eta = 1.0000$), where a one percent change in the quarantine rate only produces a decrease in $\mathcal{R}_0$ of approximately 0.6487%. This indicates that the influence of the quarantine rate on $\mathcal{R}_0$ is shared with other parameters, so its impact is relatively small compared to parameters such as the contact rate. It should be emphasized that the negative sensitivity index only indicates an inverse mathematical relationship between the quarantine rate and $\mathcal{R}_0$, and should not be interpreted as evidence that quarantine is carried out too late or is ineffective.

The disease progression rate (β) has a sensitivity index of $+0.241\%$. Mathematically, this positive value means that $\mathcal{R}_0$ is an increasing function of β, so that any increase in the disease progression rate will cause an increase in $\mathcal{R}_0$, and conversely any decrease in β will decrease $\mathcal{R}_0$. However, the relatively small magnitude of the index at $+0.241\%$ indicates that the influence of β on $\mathcal{R}_0$ is not as large as other parameters such as the contact rate (η) which has an index of $+1.0$. A one percent change in β only produces an increase in $\mathcal{R}_0$ of approximately 0.241%, whereas the same change in η produces an increase in $\mathcal{R}_0$ of one percent. Epidemiologically, this finding has profound implications. The disease progression rate (β) reflects the speed at which individuals move from the exposed stage to the infectious stage. Although this parameter is important in determining how quickly a person becomes infectious after exposure, its influence on the overall potential for disease spread is actually smaller compared to parameters that regulate the frequency of interaction between individuals (η). This indicates that the biological characteristics of the disease agent, such as the incubation period and the speed of infection development, have a more limited role in determining the magnitude of an outbreak compared to behavioral factors and population social structure. In other words, although diphtheria has a relatively short incubation period, the most determining factor in whether an outbreak will spread widely is how often susceptible individuals come into contact with

infected individuals. This finding confirms that interventions targeting the reduction of contact between individuals will have a much greater impact on reducing $\mathcal{R}_0$ compared to interventions that only target clinical aspects of the disease.

Overall, the results of this sensitivity analysis indicate that diphtheria control efforts should prioritize interventions targeting parameters with the greatest mathematical influence on $\mathcal{R}_0$, particularly reducing the contact rate (η) and significantly increasing the quarantine rate (γ) in a measurable way. Although the natural death rate (δ) shows a strong negative influence, this parameter cannot be intervened upon and only reflects demographic dynamics. Therefore, public health programs should focus on modifiable parameters, such as strengthening early detection and isolation systems, reducing contact between individuals through activity restrictions and mask use, increasing public awareness, and increasing vaccination coverage. By understanding which parameters have the most significant mathematical impact, interventions can be designed more precisely to achieve maximum effectiveness in suppressing the spread of diphtheria.

9. Parameter Estimation

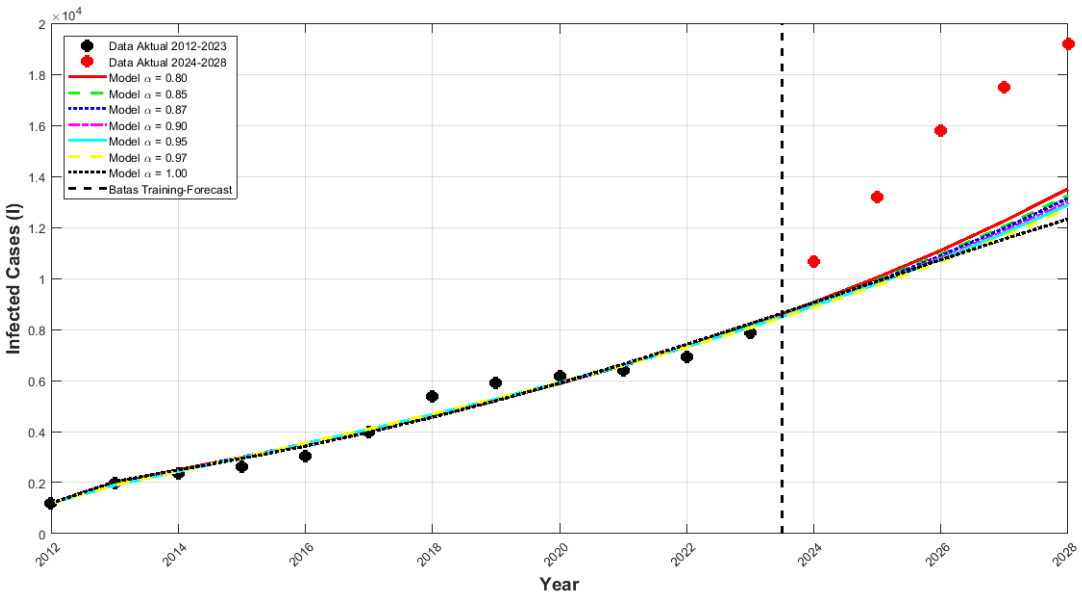

Figure 3. Parameter estimation and forecasting of diphtheria cases

Based on the parameter estimation results of the $SEIAQR$ model for diphtheria shown in Figure 3 using the fractional derivative approach, a number of values were obtained that mathematically describe how this disease spreads and how the health system responds to it. This estimation was carried out by calibrating the model against diphtheria case data from 2012 to 2023 [8]. The parameter estimation process was performed by minimizing the squared error between model predictions and actual data using a nonlinear least squares optimization algorithm. The objective function minimized is $J(\Theta) = \sum_{i=1}^{n}(y_i - \hat{y}_i(\Theta))^2$, where y_i is the actual data, $\hat{y}_i(\Theta)$ is the model prediction with parameter vector $\Theta = (\mu, \delta, \eta, \beta, \gamma, \varepsilon, \theta, \rho, w, \alpha)$, and n is the number of data points. To find the optimal parameter values, an iterative algorithm was used with a convergence criterion when the change in the objective function between two consecutive iterations was less than 10^{-6}. The fractional order α was selected by minimizing the Root Mean Square Error (RMSE) between the model and data, where $\alpha = 0.97$ yielded the best RMSE of 357.61. The quality of model fit for each fractional order is presented in Table 4, which shows

that the fractional-order model with $\alpha = 0.97$ provides a better fit compared to the integer-order model ($\alpha = 1.00$) with RMSE = 398.21. The measurable parameters provide a strong foundation for understanding the transmission mechanisms, severity levels, and the effectiveness of control efforts that have been implemented so far.

The demographic parameters, namely the natural growth rate (μ) and the natural death rate (δ), were calculated based on Indonesian demographic data and remain constant across all fractional orders α. In 2023, the population of Indonesia aged 0 to 9 years (N) was estimated at 30,395,671 and the number of births (u) was 2,805,024 [8]. Based on these data, μ is calculated as the ratio of births to total population, i.e., $\mu = \frac{u}{N} = \frac{2{,}805{,}024}{30{,}395{,}671} \approx 0.09$ per year. Meanwhile, the average life expectancy in Indonesia is 72.175 years, so δ is calculated as the reciprocal of life expectancy, i.e., $\delta = \frac{1}{72.175} \approx 0.0141$ per year. The value of μ, which appears higher than the national crude birth rate, can be attributed to the fitting procedure also accommodating factors such as population age structure or migration inflows that are not explicitly modeled within the compartmental framework, while $\delta = 0.014$ per year corresponds to a life expectancy of approximately 72.175 years. To further validate the superiority of the fractional-order model, we compared the model outputs for various fractional orders ($\alpha = 0.80, 0.85, 0.87, 0.90, 0.95, 0.97, 1.00$) against the actual diphtheria case data from 2012 to 2023 [8]. Table 3 presents the comparison results, where the values represent the cumulative number of cases predicted by the model for each year. The Root Mean Square Error (RMSE) values clearly demonstrate that the fractional-order model

Table 3. Comparison of Model Predictions with Actual Diphtheria Cases in Indonesia (2012–2023) for Various Fractional Orders α

Year	Actual Data	Fractional Order α						
		0.80	0.85	0.87	0.90	0.95	0.97	1.00
2012	1192	1192	1192	1192	1192	1192	1192	1192
2013	1970	1985	1959	1947	1930	1895	1894	2036
2014	2366	2498	2484	2477	2468	2439	2446	2499
2015	2618	3002	2999	2999	2997	2979	2992	2945
2016	3033	3516	3524	3528	3534	3526	3542	3432
2017	3987	4053	4067	4075	4086	4087	4104	3971
2018	5373	4621	4638	4648	4662	4668	4684	4563
2019	5902	5228	5244	5253	5267	5277	5288	5206
2020	6161	5879	5889	5896	5907	5918	5922	5900
2021	6396	6582	6581	6584	6588	6597	6591	6639
2022	6937	7342	7325	7321	7316	7319	7301	7417
2023	7886	8167	8127	8114	8095	8090	8058	8226
RMSE	-	385.02	375.90	372.19	366.67	361.53	**357.61**	398.21

Note: Bold value indicates the best fit (lowest RMSE).

provides a good fit to the data. Based on the RMSE values, the fractional order $\alpha = 0.97$ was selected because it provides the best balance between prediction accuracy (RMSE = 357.61) and numerical stability, while still maintaining a significant memory effect. This finding confirms that the fractional-order model captures the memory effects inherent in diphtheria transmission dynamics more effectively, leading to more accurate predictions. The following is a table of the estimated parameter values in Table 4.

Table 4. Model parameters, estimated values for $\alpha = 0.97$, sources, and units

Parameter	Value	Unit	Source
w	0.464564	-	Estimated from diphtheria data 2012-2023 [8]
μ	0.09	per year	Calculated from [8]: $\mu = \frac{u}{N}$
δ	0.0141	per year	Calculated from [8]: $\delta = \frac{1}{72.175}$
η	0.01	per day	Estimated from diphtheria data 2012-2023 [8]
β	0.043958	per day	Estimated from diphtheria data 2012-2023 [8]
γ	0.039383	per day	Estimated from diphtheria data 2012-2023 [8]
ε	0.2	per day	Estimated from diphtheria data 2012-2023 [8]
θ	0.006830	per day	Estimated from diphtheria data 2012-2023 [8]
ρ	0.4	per day	Estimated from diphtheria data 2012-2023 [8]

The estimated parameter values provide important epidemiological insights. For $\alpha = 0.97$, the parameter $w = 0.464564$ indicates that 46.5% of cases are asymptomatic. Although this proportion has the potential to enhance transmission, the basic reproduction number is $\mathcal{R}_0 = 0.3737 < 1$, meaning that the disease is extinction. This condition occurs because the memory effect, low contact rate ($\eta = 0.01$), and quarantine ($\gamma = 0.039383$) collectively suppress transmission. Global stability when $\mathcal{R}_0 < 1$ ensures that the system returns to the disease-free state as long as interventions are maintained. Therefore, control strategies must be sustained, namely maintaining high vaccination coverage and effective quarantine, because relaxing interventions could potentially increase $\mathcal{R}_0$ again.

The quarantine rate for symptomatic cases ($\gamma = 0.039383$) should not be interpreted literally as health system performance, but rather as an artifact of model identifiability limitations and data constraints, due to overlap with other transmission parameters (β, η, ρ) and limited data for compartments Q and A. The low natural recovery rate ($\varepsilon = 0.2$) and significant disease-induced death rate ($\theta = 0.006830$) confirm that diphtheria is not a self-limiting disease and requires active medical intervention, such as the availability of antitoxin, rapid detection, and healthcare worker training.

The fractional parameter $\alpha = 0.97$ reflects a strong memory effect, where past transmission events influence current dynamics. This is biologically plausible because vaccine-induced immunity has long duration, community behavior is shaped by past outbreak experiences, and the incubation period makes current transmission dependent on past conditions. The fractional approach captures the reality that diphtheria elimination depends on the accumulation of past control efforts, not only current interventions. For forecasting, predictions using $\alpha = 0.97$ are more accurate (RMSE = 357.61) than integer-order predictions (RMSE = 398.21), suggesting that memory effects should be incorporated into forecasting models.

10. Numerical Simulation

In this study, the fractional model (2) is solved numerically for various values of α, with constant parameters taken from previous studies and listed in Table 4. Simulations are conducted to observe the dynamics of infection over time, while also analyzing the effect of the recovery rate on the progression of infection under various coverage levels of intervention. To gain a deeper understanding of the outbreak dynamics, we modify the $SEIAQR$ model from integer order to fractional order using the Caputo derivative, as applied in model (2).

We recall that the general form of the fractional system is expressed as

$$D^{\alpha} X(t) = H(t, X(t)), \tag{24}$$

where $0 < \alpha \leq 1$ denotes the fractional order.

Based on Definition (2.1), equation (24) can be represented in the Volterra integral form as

$$X(t) = \sum_{j=0}^{\lceil\alpha\rceil-1} \frac{X_0^{(j)} t^j}{j!} + \frac{1}{\Gamma(\alpha)} \int_0^t (t-s)^{\alpha-1} H(s, X(s))\, ds, \tag{25}$$

which, upon integration and discretization using the predictor-corrector method, yields

$$X(t) = \sum_{j=0}^{\lceil\alpha\rceil-1} \frac{X_0^{(j)} t^j}{j!} + \frac{h^\alpha}{\Gamma(\alpha+2)} H(t_{i+1}, X^P(t_{i+1})) + \frac{h^\alpha}{\Gamma(\alpha+2)} \sum_{n=0}^{i} c_{n,i+1} H(t_n, X(t_n)), \tag{26}$$

with

$$h = \frac{T}{M}, \qquad t_i = ih, \quad i = 0, 1, 2, \ldots, M \in \mathbb{Z}^+,$$

and the predictor given by

$$X^P(t_{i+1}) = \sum_{j=0}^{\lceil\alpha\rceil-1} \frac{X_0^{(j)} t^j}{j!} + \frac{h^\alpha}{\Gamma(\alpha+1)} \sum_{n=0}^{i} d_{n,i+1} H(t_n, X(t_n)). \tag{27}$$

Using the numerical approach described above as a guideline, the proposed model can be referred to as the fractional $SEIAQR$ model solved via the predictor-corrector method. Subsequently, the discretization results of our model (2) are presented in the following equation:

$$\begin{aligned}
\begin{bmatrix} S_h(\tau_{i+1}) \\ E_h(\tau_{i+1}) \\ I_h(\tau_{i+1}) \\ A_h(\tau_{i+1}) \\ Q_h(\tau_{i+1}) \\ R_h(\tau_{i+1}) \end{bmatrix} &= \begin{bmatrix} S(0) \\ E(0) \\ I(0) \\ A(0) \\ Q(0) \\ R(0) \end{bmatrix} + \frac{h^\alpha}{\Gamma(\alpha+2)} \begin{bmatrix} F_1\big(\tau_{i+1}, S_h^P(\tau_{n+1}), E_h^P(\tau_{n+1}), I_h^P(\tau_{n+1}), A_h^P(\tau_{n+1}), Q_h^P(\tau_{n+1}), R_h^P(\tau_{n+1})\big) \\ F_2\big(\tau_{i+1}, S_h^P(\tau_{n+1}), E_h^P(\tau_{n+1}), I_h^P(\tau_{n+1}), A_h^P(\tau_{n+1}), Q_h^P(\tau_{n+1}), R_h^P(\tau_{n+1})\big) \\ F_3\big(\tau_{i+1}, S_h^P(\tau_{n+1}), E_h^P(\tau_{n+1}), I_h^P(\tau_{n+1}), A_h^P(\tau_{n+1}), Q_h^P(\tau_{n+1}), R_h^P(\tau_{n+1})\big) \\ F_4\big(\tau_{i+1}, S_h^P(\tau_{n+1}), E_h^P(\tau_{n+1}), I_h^P(\tau_{n+1}), A_h^P(\tau_{n+1}), Q_h^P(\tau_{n+1}), R_h^P(\tau_{n+1})\big) \\ F_5\big(\tau_{i+1}, S_h^P(\tau_{n+1}), E_h^P(\tau_{n+1}), I_h^P(\tau_{n+1}), A_h^P(\tau_{n+1}), Q_h^P(\tau_{n+1}), R_h^P(\tau_{n+1})\big) \\ F_6\big(\tau_{i+1}, S_h^P(\tau_{n+1}), E_h^P(\tau_{n+1}), I_h^P(\tau_{n+1}), A_h^P(\tau_{n+1}), Q_h^P(\tau_{n+1}), R_h^P(\tau_{n+1})\big) \end{bmatrix} \\
&+ \frac{h^\alpha}{\Gamma(\alpha+2)} \sum_{j=0}^{n} c_{j,i+1} \begin{bmatrix} F_1\big(\tau_j, S_h^P(\tau_j), E_h^P(\tau_j), I_h^P(\tau_j), A_h^P(\tau_j), Q_h^P(\tau_j), R_h^P(\tau_j)\big) \\ F_2\big(\tau_j, S_h^P(\tau_j), E_h^P(\tau_j), I_h^P(\tau_j), A_h^P(\tau_j), Q_h^P(\tau_j), R_h^P(\tau_j)\big) \\ F_3\big(\tau_j, S_h^P(\tau_j), E_h^P(\tau_j), I_h^P(\tau_j), A_h^P(\tau_j), Q_h^P(\tau_j), R_h^P(\tau_j)\big) \\ F_4\big(\tau_j, S_h^P(\tau_j), E_h^P(\tau_j), I_h^P(\tau_j), A_h^P(\tau_j), Q_h^P(\tau_j), R_h^P(\tau_j)\big) \\ F_5\big(\tau_j, S_h^P(\tau_j), E_h^P(\tau_j), I_h^P(\tau_j), A_h^P(\tau_j), Q_h^P(\tau_j), R_h^P(\tau_j)\big) \\ F_6\big(\tau_j, S_h^P(\tau_j), E_h^P(\tau_j), I_h^P(\tau_j), A_h^P(\tau_j), Q_h^P(\tau_j), R_h^P(\tau_j)\big) \end{bmatrix},
\end{aligned} \tag{28}$$

with the predictor values given by

$$\begin{bmatrix} S_h^P(\tau_{i+1}) \\ E_h^P(\tau_{i+1}) \\ I_h^P(\tau_{i+1}) \\ A_h^P(\tau_{i+1}) \\ Q_h^P(\tau_{i+1}) \\ R_h^P(\tau_{i+1}) \end{bmatrix} = \begin{bmatrix} S(0) \\ E(0) \\ I(0) \\ A(0) \\ Q(0) \\ R(0) \end{bmatrix} + \frac{1}{\Gamma(\alpha)} \sum_{j=0}^{n} d_{j,i+1} \begin{bmatrix} F_1\big(\tau_j, S_h(\tau_j), E_h(\tau_j), I_h(\tau_j), A_h(\tau_j), Q_h(\tau_j), R_h(\tau_j)\big) \\ F_2\big(\tau_j, S_h(\tau_j), E_h(\tau_j), I_h(\tau_j), A_h(\tau_j), Q_h(\tau_j), R_h(\tau_j)\big) \\ F_3\big(\tau_j, S_h(\tau_j), E_h(\tau_j), I_h(\tau_j), A_h(\tau_j), Q_h(\tau_j), R_h(\tau_j)\big) \\ F_4\big(\tau_j, S_h(\tau_j), E_h(\tau_j), I_h(\tau_j), A_h(\tau_j), Q_h(\tau_j), R_h(\tau_j)\big) \\ F_5\big(\tau_j, S_h(\tau_j), E_h(\tau_j), I_h(\tau_j), A_h(\tau_j), Q_h(\tau_j), R_h(\tau_j)\big) \\ F_6\big(\tau_j, S_h(\tau_j), E_h(\tau_j), I_h(\tau_j), A_h(\tau_j), Q_h(\tau_j), R_h(\tau_j)\big) \end{bmatrix}. \tag{29}$$

Let $S_h, E_h, I_h, A_h, Q_h,$ and R_h denote the corrector schemes for the susceptible, exposed, infected, asymptomatic, quarantined, and recovered individuals, respectively. Similarly, $S_h^P, E_h^P, I_h^P, A_h^P, Q_h^P,$ and R_h^P represent the corresponding predictor schemes for the same compartments.

The parameter h denotes the step size. The coefficients used in the numerical scheme are defined as follows:

$$c_{j,i+1} = \begin{cases} i^{\alpha+1} - (i-\alpha)(i+\alpha)^{\alpha}, & j = 0, \\ (i-j+2)^{\alpha+1} + (i-j)^{\alpha+1} - 2(i-j+1)^{\alpha+1}, & 1 \le j \le i, \\ 1, & j = i+1, \end{cases}$$

and

$$d_{j,i+1} = \frac{h^{\alpha}}{\alpha}((i-j+1)^{\alpha} - (i-j)^{\alpha}), \quad 0 \le j \le i.$$

The initial conditions for the simulation are $S(0) = 0.9$, $E(0) = 0.05$, $I(0) = 0.02$, $A(0) = 0.02$, $Q(0) = 0.01$, and $R(0) = 0$. The simulation is conducted over a period of 1000 days. The numerical results are presented in Figure 4 and discussed as follows.

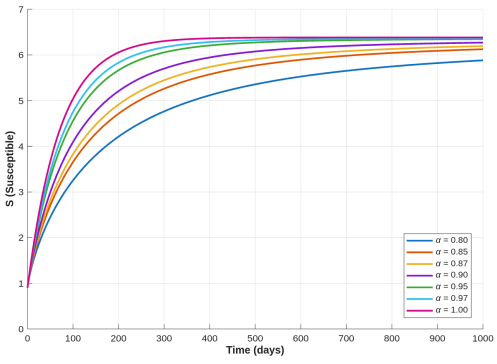

(a)

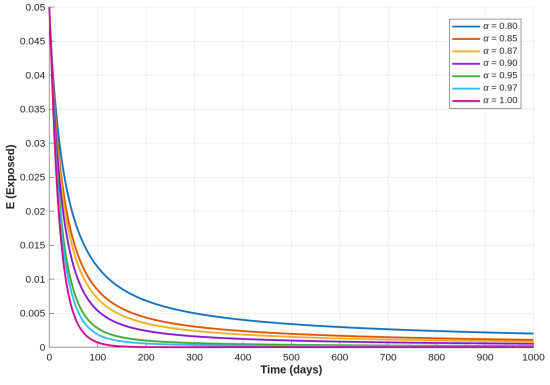

(b)

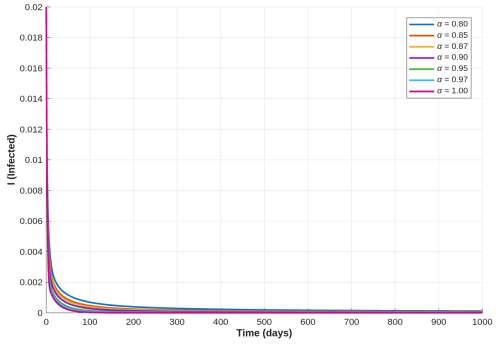

(c)

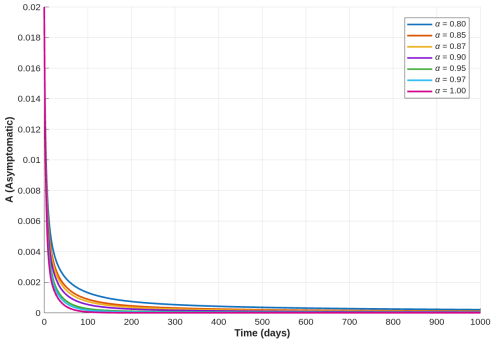

(d)

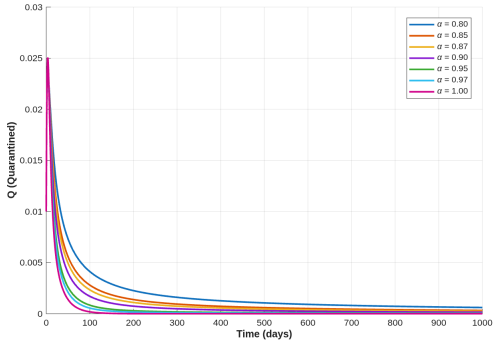

(e)

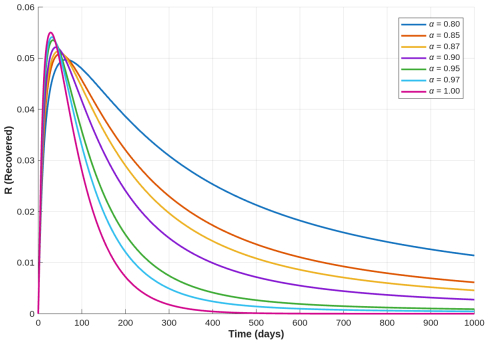

(f)

Figure 4. Numerical simulation are illustrated which represent the dynamics of S, E, I, A, Q, R at infection-free steady state for various values of fractional derivative α, with $\mathcal{R}_0 < 1$.

Numerical simulations are performed for various fractional orders: $\alpha = 0.80, 0.85, 0.87, 0.90, 0.95, 0.97,$ and 1.00. The selection of this range of α values aims to demonstrate the influence of memory effects on the transmission dynamics of diphtheria, where smaller values of α represent stronger memory effects. The condition of $\mathcal{R}_0 < 1$, the susceptible population exhibits a consistent increase throughout the simulation period for all values of the fractional order α shown in the Figure 4a. This increase occurs because the low transmission rate fails to generate a significant epidemic, so individuals remain in the susceptible compartment without transitioning to exposed or infected compartments. The birth rate $\mu = 0.09$ per year exceeds the natural death rate $\delta = 0.0141$ per year, resulting in the accumulation of susceptible individuals over time. The memory effect represented by smaller fractional orders $(\alpha < 1)$ slows the rate of increase in the susceptible population compared to the integer-order model $(\alpha = 1.00)$. At day 1000, for $\alpha = 0.80$, the susceptible population reaches approximately 5.8, whereas for $\alpha = 1.00$, it reaches approximately 6.2. This difference indicates that the fractional model provides a more conservative estimate than the integer model. The continuous growth of the susceptible population suggests that any relaxation of interventions may trigger a new wave of transmission. Vaccination programs should not be discontinued even as cases decline significantly. The growing susceptible population represents potential fuel for future outbreaks if interventions are relaxed. The government must maintain high vaccination coverage and continuously monitor the dynamics of the susceptible population, particularly among children who are the primary targets of the diphtheria immunization program.

Figure 4b shows the dynamics of the exposed population (E) over 1000 days of simulation for various fractional order. The exposed population shows a consistent decline throughout the simulation period for all values of α. The condition of $\mathcal{R}_0 < 1$, each exposed individual does not progress to a significant infection case and eventually recovers without transmitting the disease. The rate of decline in the exposed population is strongly influenced by the value of α. At day 1000, for $\alpha = 0.80$, the exposed population remains around 0.0025, while for $\alpha = 1.00$, it has declined to near zero. A stronger memory effect (smaller α) slows the decline of the exposed population, meaning that exposed individuals remain longer in this compartment when memory effects are considered. The longer individuals stay in the exposed phase, the greater the chance they may progress to infection cases if interventions are relaxed. The fractional model warns that the decline in exposed cases is slower than estimated by the integer model, so surveillance of the exposed population must be maintained even as infection cases begin to decline. Aggressive contact tracing and early isolation of exposed individuals remain essential despite the low transmission rate. Exposed individuals who persist longer in the population remain potential sources of transmission. The epidemiological surveillance system must have the capacity to detect and isolate exposed individuals quickly, especially in populations with strong memory characteristics such as communities with high adherence to health protocols based on previous outbreak experiences.

Figure 4c shows the dynamics of the symptomatic infected population (I) over 1000 days of simulation for various fractional order values $\alpha = 0.7; 0.8; 0.9;$ and 1.0. The symptomatic infected population exhibits a sharp

decline at the beginning of the simulation for all values of the fractional order α, decreasing from the initial value of 0.02 to near zero by day 1000. The differences among α values are not substantial in this compartment, as the disease no longer spreads effectively under the condition $\mathcal{R}_0 < 1$, leading all models to predict rapid disease extinction. A slightly slower decline is observed for $\alpha = 0.80$ compared to $\alpha = 1.00$, indicating that the memory effect marginally slows the reduction of symptomatic cases. Symptomatic cases disappear quickly when $\mathcal{R}_0 < 1$, resulting in a significant reduction in hospital burden and the demand for intensive care within a short period. However, this rapid decline should not lead to complacency among the public and policymakers. Evidence from various outbreaks demonstrates that a swift decrease in cases is often followed by a second wave if interventions are relaxed prematurely. Although symptomatic cases decline rapidly, the healthcare system must maintain preparedness to manage cases arising from undetected asymptomatic transmission. The availability of diphtheria antitoxin, antibiotics, and intensive care facilities must be sustained, as diphtheria has a high severity level and can be fatal if not treated promptly.

Figure 4d shows the dynamics of the asymptomatic population (A) over 1000 days of simulation for various fractional order values α. The asymptomatic population shows a decline pattern that is strongly influenced by the value of α. For $\alpha = 0.80$, the asymptomatic population declines from the initial value of 0.02 to approximately 0.0015 at day 1000, while for $\alpha = 1.00$, it declines to near zero. The memory effect has the most significant influence on the asymptomatic compartment compared to other compartments. Asymptomatic individuals persist longer in the population when memory effects are considered, meaning they continue to have the potential to transmit disease undetected for a longer period. Asymptomatic individuals are hidden sources of transmission because they do not show symptoms and do not seek treatment, allowing them to continue transmitting the disease without identification. The fractional model warns that the decline in asymptomatic cases is slower than estimated by the integer model, so surveillance strategies must include mass testing and aggressive contact tracing, even when symptomatic cases have begun to decline. The substantial proportion of asymptomatic cases ($w = 0.464564$ or 46.5% of cases are asymptomatic) further emphasizes the importance of early detection of asymptomatic cases.

Figure 4e shows the dynamics of the quarantined population (Q) over 1000 days of simulation for various fractional order values α, the quarantined population exhibits an initial increase followed by a gradual decline, reflecting that a number of infected individuals enter quarantine in the early phase, but as infection cases decline, the number of individuals entering quarantine also decreases. The integer model ($\alpha = 1.00$) shows a quarantined population that remains constant throughout the simulation period, which is epidemiologically unrealistic because it assumes that the number of quarantined individuals does not change even as infection cases continue to decline. The fractional model is more realistic because it captures the dynamics that quarantine should decrease as cases decline. The quarantine system must be maintained even as cases begin to decline to prevent disease resurgence. Quarantine capacity can be gradually adjusted as cases decline so that resources can be allocated efficiently. The government must ensure that quarantine facilities remain available and that quarantine procedures are carried out with discipline, especially for new cases that may arise from asymptomatic transmission.

Figure 4f shows the dynamics of the recovered population (R) over 100 days of simulation for various fractional order values α. The recovered population reaches its peak around day 50 for all values of α, after which it declines at different rates until day 1000. For $\alpha = 0.80$ and 0.85, the recovered population decreases consistently from 0.048-0.050 to 0.005-0.013, indicating that the proportion of recovered individuals relative to the total population diminishes as the population continues to grow through births and migration. The fractional-order models with $\alpha = 0.80$, 0.85, 0.90, and 0.95 provide realistic dynamics of the recovered population, exhibiting gradual declines or stabilizations at low levels. In contrast, the integer-order model ($\alpha = 1.00$) fails to capture the proportional dynamics because it neglects memory effects. These findings emphasize the importance of fractional-order models, particularly $\alpha = 0.90$ or 0.95, for policy planning. The government must maintain medical logistics, booster vaccination programs, and public education campaigns, and should not interpret high recovery rates as an indication that the disease is fully under control.

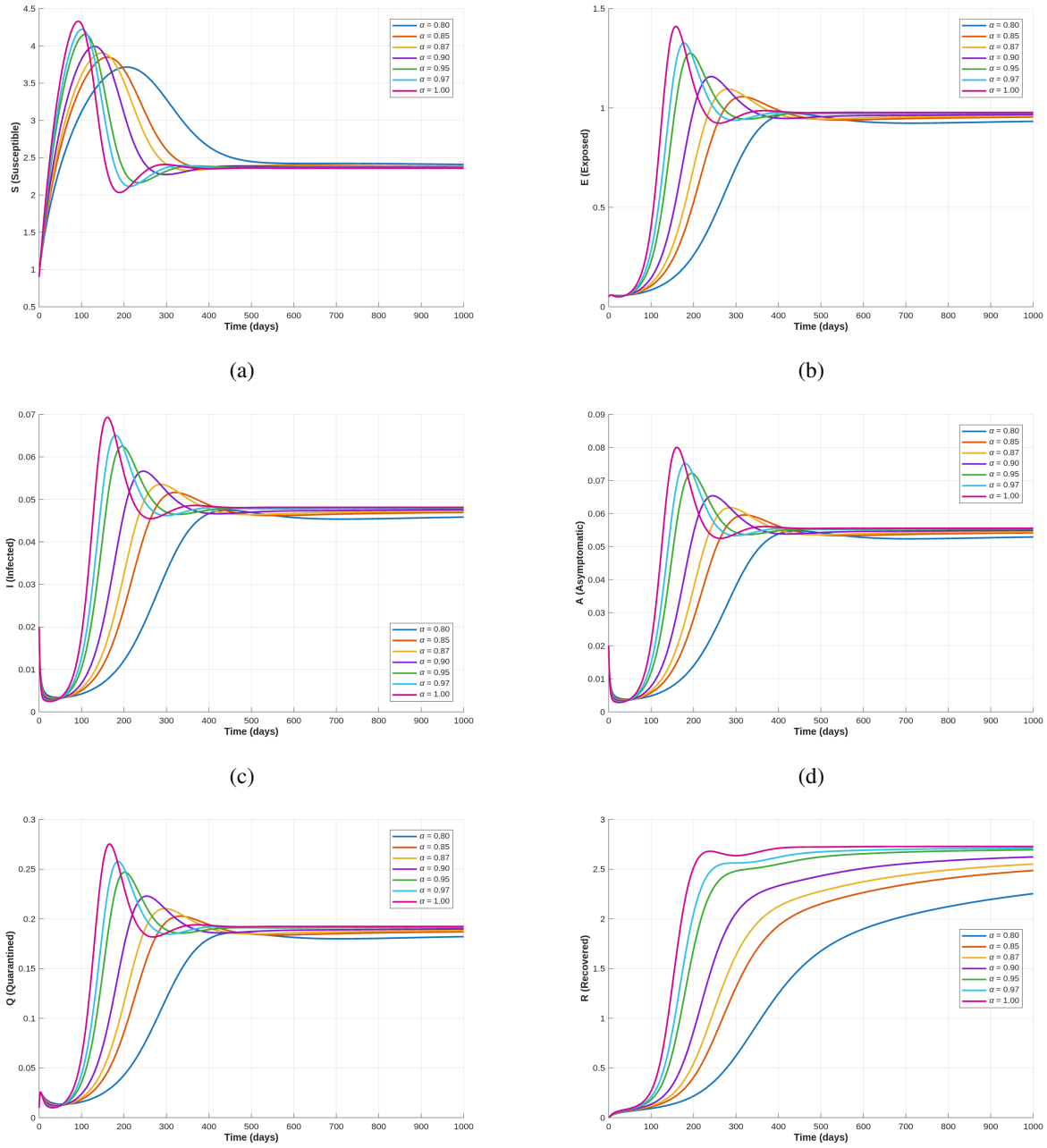

Figure 5. Numerical simulation are illustrated which represent the dynamics of S, E, I, A, Q, R at infection-present steady state for various values of fractional derivative α, with $\mathcal{R}_0 > 1$.

Based on the analysis of Figure 5, which illustrates the dynamics of the $SEIAQR$ model under the condition $\mathcal{R}_0 > 1$ (endemic), it is evident that each population compartment exhibits distinct behavior, reflecting serious challenges in controlling diphtheria outbreaks. Simulations were conducted for various fractional order values, namely $\alpha = 0.8; 0.85; 0.87; 0.9; 0.95; 0.97;$ and 1.0 (integer-order model), with the aim of demonstrating the influence of memory effects on disease transmission dynamics.

Figure 5a for the susceptible population (S) shows a consistent increase over time for all fractional order values (α). On day 100, the susceptible population increases from 0.9 to approximately 3.75 for $\alpha = 0.8$; 3.85 for $\alpha = 0.85$; 4.00 for $\alpha = 0.9$; and 4.30 for the integer-order model ($\alpha = 1.0$). This increase is primarily driven by the birth rate ($\mu = 0.09$ per year) being higher than the natural death rate ($\delta = 0.0141$ per year). Consequently, even though the disease is actively spreading, the susceptible population continues to grow. The smaller the value of α, the slower the increase, because the memory effect slows down changes in population dynamics. This indicates that the government must continuously increase vaccination coverage just to "catch up" with the growth of the new susceptible population.

Figure 5b for the exposed population (E) shows a highly varied pattern depending on the value of α. For $\alpha = 0.8$ and 0.85, the exposed population remains constant at 0.05 throughout the 100-day simulation. This means that the strong memory effect successfully suppresses the transmission rate, so the number of individuals moving from susceptible to exposed does not increase significantly, although transmission still occurs at a low level requiring continuous monitoring. For $\alpha = 0.9$, the exposed population gradually increases from 0.05 to 0.15 on day 100, reflecting that transmission begins to occur at a moderate rate as the memory effect weakens. Meanwhile, for the integer-order model ($\alpha = 1.0$), the exposed population increases very rapidly at the beginning of the simulation, indicating that without memory effects, transmission occurs very quickly but then reaches a saturation point due to the limited available susceptible population, thus requiring rapid and aggressive intervention to suppress case surges.

Figure 5c for the symptomatic infected population (I) shows fluctuations and a tendency to increase for several values of α, although not as drastic as the integer-order model. In the early days, all curves start from the same point. For $\alpha = 0.8$ and 0.85, the symptomatic infected population shows a slow initial decline and then tends to stabilize at a low level. Meanwhile, for $\alpha = 0.9$ and 1.0, this population shows a clearer increase, with the integer-order model reaching a higher and faster peak. This indicates that an outbreak will occur with a possibly lower peak in the fractional model, but the outbreak duration could be longer because the memory effect slows down the transmission and recovery processes. Consequently, the burden on the healthcare system may be more prolonged even though it does not reach as high a peak as predicted by the integer-order model.

Figure 5d for the asymptomatic population (A) shows a consistent increase over time, especially for higher values of α. This asymptomatic population is very important because asymptomatic individuals do not show signs of illness and therefore do not seek treatment, but they can still transmit the disease silently. The graph shows that for $\alpha = 0.9$ and above, the asymptomatic population increases significantly, meaning they become hidden sources of transmission that are difficult to detect. This requires the government to expand mass testing programs and aggressive contact tracing to identify and isolate asymptomatic individuals, because failure to detect them can lead to sustained transmission that triggers subsequent outbreak waves.

Figure 5e for the quarantined population (Q) shows a highly informative pattern. In the fractional model, the quarantined population increases at the beginning of the outbreak as the number of detected cases increases, then gradually decreases as cases become controlled. This pattern reflects realistic dynamics, in contrast to the integer-order model which shows a constant quarantined population, which does not reflect actual conditions. These fluctuations indicate that quarantine capacity must always be available and ready to be activated at any time. The government needs to ensure that quarantine facilities and isolation procedures continue to function properly even though cases show a downward trend, because premature relaxation of quarantine can trigger a resurgence of the outbreak.

Figure 5f for the recovered population (R) shows an increase at the beginning of the simulation as a result of the recovery process of infected individuals, reflecting the effectiveness of treatments such as antitoxin and antibiotic administration. However, after reaching its peak around day 200, the proportion of the recovered population to the total population tends to decrease because the total population continues to increase through births, although the absolute number of recovered individuals may remain. This reminds us that treatment success should not make the public complacent. The government must continue to ensure access to quality healthcare, as well as maintain educational campaigns about the importance of early treatment and adherence to health protocols, to prevent future disease resurgence.

Overall, Figure 5 confirms that under the condition $\mathcal{R}_0 > 1$, diphtheria becomes endemic and requires a sustained intervention strategy. The government should focus efforts on reducing the contact rate (η), increasing quarantine (γ), early detection of asymptomatic cases through mass testing, as well as massive and continuous vaccination. The fractional model provides a warning that control policies must be long-term because the memory effect slows down the population's response to policy changes, so premature relaxation of interventions can trigger a resurgence of the outbreak.

11. Discussion

This study develops and analyzes a fractional $SEIAQR$ epidemiological model to understand the transmission dynamics of diphtheria in Indonesia, with a focus on the influence of memory effects represented by the fractional order parameter (α). The main findings demonstrate that the fractional model with $\alpha = 0.97$ provides the most accurate predictions (RMSE = 357.61) compared to the integer-order model ($\alpha = 1.00$, RMSE = 398.21), indicating that memory effects play a significant role in diphtheria transmission dynamics. Based on parameter estimation, it was found that 46.5% of cases are asymptomatic with a low contact rate ($\eta = 0.01$) and quarantine rate ($\gamma = 0.039$) that collectively suppress the basic reproduction number ($\mathcal{R}_0 = 0.3737 < 1$), resulting in disease extinction as long as interventions are maintained. Stability analysis confirms that the disease-free equilibrium is globally stable when $\mathcal{R}_0 < 1$, while the endemic equilibrium is stable when $\mathcal{R}_0 > 1$, reinforced by sensitivity analysis identifying the contact rate (η), quarantine rate (γ), and proportion of symptomatic cases (w) as the most influential parameters on $\mathcal{R}_0$.

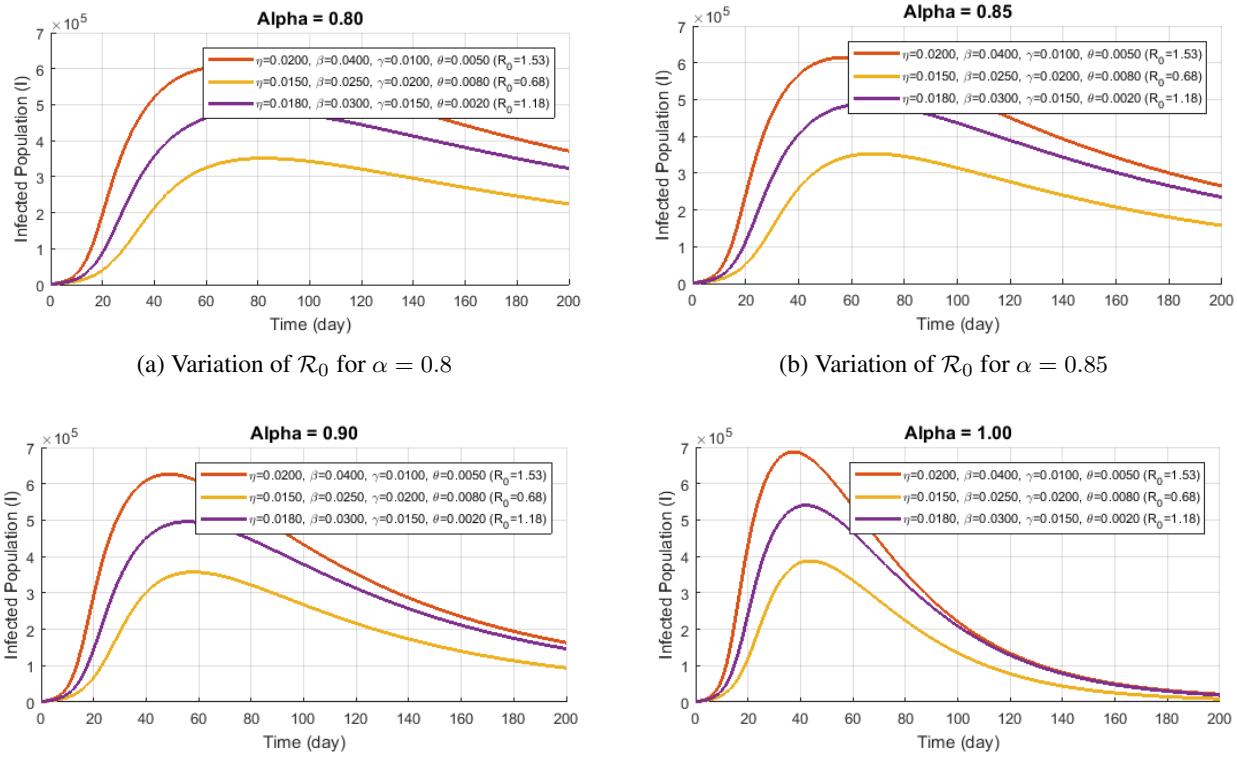

(a) Variation of $\mathcal{R}_0$ for $\alpha = 0.8$

(b) Variation of $\mathcal{R}_0$ for $\alpha = 0.85$

(c) Variation of $\mathcal{R}_0$ for $\alpha = 0.9$

(d) Variation of $\mathcal{R}_0$ for $\alpha = 1$

Figure 6. Numerical solutions of model $SEIAQR$ showing the infected subpopulation (I) with variations in $\mathcal{R}_0$ for different values of α.

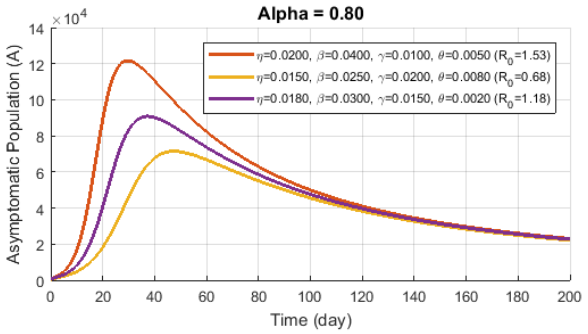

(a) Variation of $\mathcal{R}_0$ for $\alpha = 0.8$

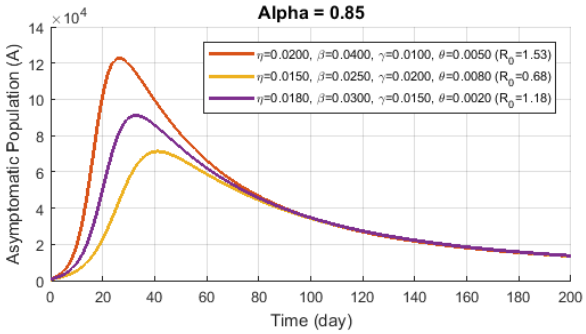

(b) Variation of $\mathcal{R}_0$ for $\alpha = 0.85$

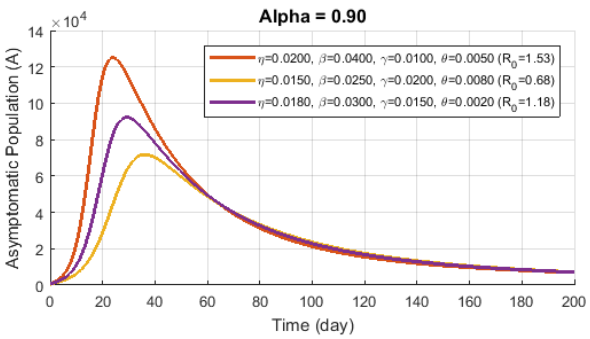

(c) Variation of $\mathcal{R}_0$ for $\alpha = 0.9$

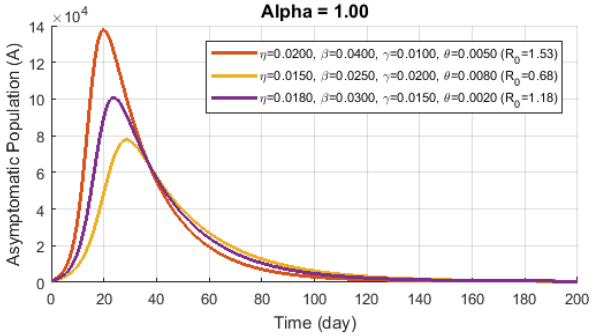

(d) Variation of $\mathcal{R}_0$ for $\alpha = 1$

Figure 7. Numerical solutions of model $SEIAQR$ showing the asymptomatic subpopulation (A) with variations in $\mathcal{R}_0$ for different values of α.

Numerical analysis of the infected and asymptomatic populations presented in Figure 6 and Figure 7 reveals significant differences across various fractional order values with important epidemiological implications. In the model with strong memory effects ($\alpha = 0.8$), the asymptomatic population exhibits a very slow and stable declining trend, where asymptomatic individuals persist longer in the population and continue to potentially transmit the disease silently even though transmission should epidemiologically be declining. Conversely, in the integer-order model ($\alpha = 1.0$), the asymptomatic population declines very rapidly, indicating that the integer-order model provides overly optimistic estimates of the speed of asymptomatic case decline. The infected population at $\alpha = 0.8$ shows almost no increase even when $\mathcal{R}_0 > 1$, while at $\alpha = 1.0$ it shows a sharp increase followed by rapid decline, reflecting aggressive but short-lived outbreak dynamics. Graphical interpretation confirms that the asymptomatic population has longer persistence than the infected population across all α values, as seen from the consistently flatter asymptomatic decline curves, confirming that asymptomatic individuals are dangerous hidden sources of transmission requiring early detection through mass testing and aggressive contact tracing as control priorities.

This study is closely related to Ghani et al. (2023) [30], who developed a fractional $SEIQR$ model for diphtheria and found $\alpha = 0.8$ as the optimal order with RMSE 0.0026, differing from our finding of $\alpha = 0.97$ with RMSE 357.61 due to differences in model structure between $SEIAQR$ and $SEIQR$, data range, and parameter complexity. Nevertheless, both studies agree that fractional models provide better prediction accuracy than integer-order models, with vaccination and treatment as the most effective interventions. The novelty of our research lies in the use of the $SEIAQR$ model that separates asymptomatic and symptomatic populations, calibration with 12 years of Indonesian diphtheria data, sensitivity analysis with 95% confidence intervals, and discussion of epidemiological implications of memory effects on the asymptomatic population based on graphical interpretation. Limitations include dependence on data quality potentially containing reporting bias, assumption of constant parameters, model identifiability limitations, and lack of consideration of spatial heterogeneity and optimal control strategies.

Policy recommendations include prioritizing contact rate reduction (η) through activity restrictions, mask use, and public awareness campaigns; strengthening early detection of asymptomatic cases through mass testing and aggressive contact tracing; sustaining vaccination programs to offset susceptible population growth; implementing long-term control policies given that memory effects slow population response; and maintaining availability of diphtheria antitoxin, antibiotics, and intensive care facilities. For future research, the use of the Atangana-Baleanu fractional derivative operator will be a primary focus due to its non-local and non-singular kernel that more accurately models biological systems with memory and heredity, providing better accuracy with lower computational cost. Additionally, recommended future directions include developing models with time-dependent parameters, incorporating spatial data, optimal control analysis, consideration of population age structure, studies on asymptomatic transmission mechanisms, and integration with real-time health surveillance systems for more accurate outbreak prediction and faster policy response.

12. Conclusion

This paper aimed to numerically examine a nonlinear fractional $SEIAQR$ epidemic model. The analysis effectively established the well-posedness, positivity, and boundedness of the solutions for this fractional $SEIAQR$ framework, and identified two equilibrium states: the disease-free equilibrium and the endemic equilibrium. The basic reproduction number ($\mathcal{R}_0$) was derived to examine the theoretical and numerical behavior of the model, where the disease-free equilibrium remains locally asymptotically stable only when $\mathcal{R}_0 < 1$, whereas the endemic equilibrium exists solely when $\mathcal{R}_0 > 1$. The study also explored the effect of various parameters on $\mathcal{R}_0$ and assessed disease transmission dynamics across different fractional orders, observing that reducing the fractional parameter from 1 led to a progressive decline in the susceptible, infected, and recovered populations. The numerical simulations in this study employed the Adams-Bashforth-Moulton predictor-corrector method, which effectively captures the memory effects inherent in the Caputo fractional derivative framework. The fractional order $\alpha = 0.97$ was identified as the optimal choice, providing the best fit to Indonesian diphtheria data from 2012 to 2023 with RMSE 357.61, outperforming the integer-order model ($\alpha = 1.00$, RMSE 398.21). These findings provide quantitative insights into the transmission dynamics of diphtheria. While the present study does not propose specific implementable control strategies, the results offer a theoretical foundation for designing future intervention policies, such as vaccination and quarantine, and may serve as a useful reference for health officials and policymakers. Future research will develop the model by comparing the Atangana-Baleanu fractional derivative operator, which features a non-local and non-singular kernel based on the Mittag-Leffler function that has been shown to provide superior accuracy and lower computational cost, and will determine optimal control strategies for hospitalization, vaccination, and quarantine interventions to achieve more effective disease containment.

Acknowledgement

The author would like to express deepest gratitude for the financial support provided through the Indonesia Bangkit Scholarship – Education Fund Management Institution (LPDP) – Ministry of Religious Affairs of the Republic of Indonesia with registration number REG20250519017. This support has been invaluable in supporting and completing this research.

REFERENCES

1. WHO, *Diphtheria*, 2024. [Online]. Available: https://www.who.int/nws-room/questions-and-answers/item/diphtheria.
2. Ministry of Health of the Republic of Indonesia, *Guidelines for Prevention and Control of Diphtheria*, 2024. [Online]. Available: https://sehatnegeriku.kemkes.go.id/wp-content/uploads/2018/01/buku-pedoman-pencegahan-dan-penanggulangan-difteri.pdf.

3. Centers for Disease Control and Prevention, *About Diphtheria*, What it is, 2025. Available: https://www.cdc.gov/diphtheria/about/causes-transmission.html.
4. National Health Service, *Diphtheria*, 2024. [Online]. Available: https://www.nhs.uk/conditions/diphtheria/.
5. Anderson, *What to Know About Diphtheria*, WebMD, 2024. [Online]. Available: https://www.webmd.com/a-to-z-guides/what-to-know-diphtheria-causes.
6. K. Rodgers, *Diphtheria*, The Editors of Encyclopaedia Britannica, Britannica, 2024. [Online]. Available: https://www.britannica.com/science/diphtheria.
7. S. R. Lamichhane, *Diphtheria*, StatPearls, 2024. [Online]. Available: https://www.ncbi.nlm.nih.gov/books/NBK560911/.
8. Ministry of Health of the Republic of Indonesia, *Indonesian Health Profile 2023*, 2024. [Online]. Available: https://kemkes.go.id/id/category-download/profil-kesehatan.
9. T. Witelski and M. Bowen, *Methods of Mathematical Modelling: Continuous Systems and Differential Equations*, Springer Cham, Switzerland, 2015.
10. F. Brauer and C. Castillo-Chavez, *Epidemic Models*, In:Mathematical Models in Population Biology and Epidemiology, Springer, New York, 2008.
11. W. Kermack and A. McKendrick, *A Contribution to The Mathematical Theory of Epidemics*, Proceedings of the Royal Society of London, vol. 115, no. 772, pp. 700–721, Aug. 1927.
12. H. Hethcote, *Three Basic Epidemiological Models*, Applied Mathematical Ecology, Biomathematics, Springer, Berlin, Heidelberg. 1989.
13. G. Puspita, M. Kharis, and Supriyono *Pemodelan Matematika pada Penyebaran Penyakit Difteri dengan Pengaruh Karantina dan Vaksinasi*, UNNES Journal of Mathematics, vol. 6, pp. 25-35, 2017.
14. M. Torrea, J. L. Torrea and D. Ortega, *A modeling of a Diphtheria epidemic in the refugees camps*, bioRxiv, Oct. 2017.
15. K. Sornbundit, W. Triampo and C. Modchang, *Mathematical modeling of diphtheria transmission in Thailand*, Computers in Biology and Medicine, vol. 87, pp. 162–168, Aug. 2017.
16. F. Ilahi and A. Widiana, *The effectiveness of vaccine in the outbreak of diphtheria: Mathematical model and simulation*, IOP Conference Series: Materials Science and Engineering, vol. 434, no. 1, Nov. 2018.
17. I. S. Fauzi et al., *Assessing the impact of booster vaccination on diphtheria transmission: Mathematical modeling and risk zone mapping*, Infectious Disease Modelling, vol. 9, pp. 245–262, Mar. 2024.
18. S. O. Adewale, S. O. Ajao, I. A. Olopade, G. A. Adeniran, and I. T. Mohammed, *Mathematical Analysis of Quarantine on the Dynamical Transmission of Diphtheria Disease Solving Riccati Equation Using Adomian Decomposition Method*, Int. J. Sci. Eng. Investig, vol. 6, pp. 8–17, 2017.
19. N. Izzati, A. Andriani, and R. Robi'aqolbi, *Optimal Control of Diphtheria Epidemic Model with Prevention and Treatment*, Journal of Physics: Conference Series, vol. 1663, no. 1, Oct. 2020.
20. N. Rahmi and M. I. Pratama, *Model Analysis of Diphtheria Disease Transmission with Vaccination, Quarantine, and Hand-Washing Behavior*, JTAM (Jurnal Teori dan Aplikasi Matematika), vol. 7, no. 2, pp. 462–473, 2023.
21. C. E. Madubueze, K. A. Tijani, and Fatmawati, *A Deterministic Mathematical Model for Optimal Control of Diphtheria Disease with Booster Vaccination*, Healthcare Analytics, vol. 4, 2023.
22. M. Sholeh, *Stability Analysis of the SIQR Model of Diphtheria Disease Spread and Migration Impact*, Barekeng: Journal of Mathematics and Its Application, vol. 19, no. 1, pp. 173-184, Jan. 2025.
23. C. W. Chukwu, Fatmawati, M. I. Utoyo, A. Setiawan, and J. O. Kanni, *Fractional Model of HIV Transmission on Workplace Productivity Using Real Data from Indonesia*, Mathematics and Computers in Simulation, vol. 225, pp. 1–15, 2024.
24. O. J. Peter, N. D. Fahrani, Fatmawati, Windarto, and C. W. Chukwu, *A Fractional Derivative Modeling Study for Measles Infection with Double Dose Vaccination*, Healthcare Analytics, vol. 4, Dec. 2023.
25. D. Belanu, M. Hassan Abadi, A. Jajarmi, K. Zarghami Vahid, and J. J. Nieto, *A New Comparative Study on the General Fractional Model of COVID-19 with Isolation and Quarantine Effects*, Alexandria Engineering Journal, vol. 61, no. 6, pp. 4779–4791, Jun. 2022.
26. M. Caputo and M. Fabrizio, *A New Definition of Fractional Derivative without Singular Kernel*, Progress in Fractional Differentiation and Applications, vol. 1, no. 2, 73-85, 2015.
27. A. Atangana and D. Baleanu, *New Fractional Derivatives with Non-Local and Non-Singular Kernel: Theory and Application to Heat Transfer Model*, Thermal Sci, vol. 20, pp. 763–769, 2016.
28. Trisilowati, I. Darti, R. R. Musafir, M. Rayungsari, and A. Suryanto, *Dynamics of a Fractional-Order COVID-19 Epidemic Model with Quarantine and Standard Incidence Rate*, Axioms, vol. 12, no. 6, 591, 2023.
29. A. Shakeel, S. Ullah and R. Faiza tul, *Numerical Computations of Fractional Differential Equations in Engineering using the Polynomial Least Squares Method*, Journal of Prime Research in Mathematics, vol. 2, pp. 13–24, 2025.
30. M. Ghani, I. Q. Utami, F. W. Triyayuda, M. Afifah, and A. Suryanto, *A Fractional SEIQR Model on Diphtheria Disease*, Modeling Earth Systems and Environment, vol. 9, no. 2, pp. 2199–2219, Jun. 2023.
31. K. Diethelm, *The Analysis of Fractional Differential Equations: An Application-Oriented Exposition Using Differential Operators of Caputo Type*, Springer, Springer Berlin, Heidelberg, 2010.
32. Y. Li, Y. Q. Chen and I. Podlubny, *Stability of fractional-order nonlinear dynamic systems: Lyapunov direct method and generalized Mittag-Lefer stability*, Comput. Math. Appl, vol. 59, n0. 5, pp. 1810–1821, Mar. 2010.
33. H. L. Li, L. Zhang, C. Hu, Y. L. Jiang and Z. Teng, *Dynamical analysis of a fractional-order predator-prey model incorporating a prey refuge*, Journal of Applied Mathematics and Computing, vol. 54, pp. 435–449, May. 2017.
34. W. Saleh and A. Kilieman, *Note on the fractional Mittag-Lefer functions by applying the modified Riemann-Liouville derivatives*, Boletim da Sociedade Paranaense de Matemática, vol. 40, pp. 45–52, 2022.
35. Z. M. Odibat and N. T. Shawagfeh, *Generalized Taylor's formula*, Comput. Appl. Math, vol. 186, no. 1, pp. 286–293, Mar. 2007.
36. C. Vargas-De-Leon, *Volterra-type Lyapunov function for fractional-order epidemic systems*, Communications in Nonlinear Science and Numerical Simulation, vol. 24, pp. 75–85, Jul. 2015.
37. J. Huo, H. Zhao and L. Zhu, *The effect of vaccines on backward bifurcation in a fractional order HIV model*, Nonlinear Analysis: Real World Applications, vol. 26, pp. 289–305, Dec. 2015.

38. K.M. Owolabi, A. Atangana, *Spatiotemporal Dynamics of Fractional Predator–Prey System with Stage Structure for the Predator*, International Journal of Applied and Computational Mathematics, vol. 3, pp. 903–924, Jul. 2017.
39. S. K. Choi, B. Kang and N. Koo, *Stability for caputo fractional differential systems*, Abstrac and Applied Analysis, vol. 2014, no. 1, 2014.
40. P. F. Hsieh and Y. Sibuya, *Basic Theory of Ordinary Differential Equations*, Universitext, Springer-Verlag, New York, 1999.
41. D. Matignon, *Stability results on fractional differential equations to control processing*, in: Proceedings of the 1996 IMACS multiconference on computational engineering in systems and application multiconference, Lille, France, vol. 2,PP. 963–968,1996.
42. I. Petras, *Fractional-Order Nonlinear Systems, Modeling, Analysis and Simulation*, Higher Education Press, Beijing, 2011.
43. M. Farman, A. Shehzad, A. Akgul, D. Baleanu, and M. Sen, *Modelling and analysis of a measles epidemic model with the constant proportional Atangana-Baleanu derivative operator*, Symmetry, vol. 15, no. 2, Feb. 2023.
44. J. P. La Salle, *The stability of dynamical systems*, Society for Industrial and Applied Mathematics, 1976.